AGU PUBLICATIONS

Geophysical Research Letters

RESEARCH LETTER
10.1002/2016GL071587

Key Points:
- Ocean model is forced with air-sea fluxes from CMIP5 models to examine the drivers of uncertainty in ocean circulation and heat uptake (OHU)
- High-latitude air-sea fluxes are the dominant source of uncertainty in the spread of Atlantic MOC and OHU over model structural uncertainty
- Subgrid-scale parameters lead to large uncertainty in the circulation and OHU, especially in the Pacific and Southern Oceans

Supporting Information:
- Table S1 and Figures S1–S11

Correspondence to:
L. Zanna,
laure.zanna@physics.ox.ac.uk

Citation:
Huber, M. B., and L. Zanna (2017), Drivers of uncertainty in simulated ocean circulation and heat uptake, *Geophys. Res. Lett.*, *44*, doi:10.1002/2016GL071587.

Received 13 OCT 2016
Accepted 17 JAN 2017
Accepted article online 19 JAN 2017

Drivers of uncertainty in simulated ocean circulation and heat uptake

Markus B. Huber[1] **and Laure Zanna**[1]

[1] Department of Physics, University of Oxford, Oxford, UK

Abstract The impact of uncertainties in air-sea fluxes and ocean model parameters on the ocean circulation and ocean heat uptake (OHU) is assessed in a novel modeling framework. We use an ocean-only model forced with the simulated sea surface fields of the CMIP5 climate models. The simulations are performed using control and 1% CO_2 warming scenarios. The ocean-only ensemble adequately reproduces the mean Atlantic Meridional Overturning Circulation (AMOC) and the zonally integrated OHU. The ensemble spread in AMOC strength, its weakening, and Atlantic OHU due to different air-sea fluxes is twice as large as the uncertainty range related to vertical and mesocale eddy diffusivities. The sensitivity of OHU to uncertainties in air-sea fluxes and model parameters differs vastly across basins, with the Southern Ocean exhibiting strong sensitivity to air-sea fluxes and model parameters. This study clearly demonstrates that model biases in air-sea fluxes are one of the key sources of uncertainty in climate simulations.

1. Introduction

The exchange of momentum, heat, freshwater, and carbon between the atmosphere and the ocean via air-sea fluxes is of fundamental importance for the Earth's climate. The magnitude and geographical distribution of these air-sea interactions have important implications for the energetics and dynamics of the ocean and its circulation [*Ferrari and Wunsch*, 2008]. For example, the knowledge of the surface heat fluxes allows to infer the oceanic meridional heat transport [*Trenberth et al.*, 2001] as well as to quantify the rate of water mass transformation [*Walin*, 1982]. Thus, the accurate quantification of the surface momentum and buoyancy fluxes in observations and climate models appears to be crucial for understanding and simulating the ocean circulation and its response to anthropogenic greenhouse gas emissions.

However, despite the importance of the air-sea fluxes both in steady state and under transient climate change there are significant long-standing uncertainties and biases in observational estimates and reanalysis products. *Valdivieso et al.* [2015] showed that most reanalysis products feature a bias during the period 1993–2009 in the global-mean net surface flux in the order of 1–2 W/m^2 which is larger than the energy gain derived from estimates of the top of atmosphere (TOA) imbalance of about 0.50 ($\pm$0.43) W/m^2 [*Loeb et al.*, 2012]. For comparison, the current generation of climate models of the Coupled Model Intercomparison Project Phase 5 (CMIP5) exhibits an uncertainty in the net surface and TOA fluxes in the order of 10 W/m^2 and 5 W/m^2, respectively [*Wild et al.*, 2015]. However, the extent to which these uncertainties in simulated air-sea fluxes impact the ocean circulation and ocean heat uptake (OHU) in climate models is not fully understood.

Previous studies assessed the impact of physical parameterizations and numerics in ocean models on the steady state ocean circulation in the North Atlantic and the Southern Oceans. Using a standard set of atmospheric fields to force different ocean-only models for the period 1948–2007, the Atlantic meridional overturning transport at 26.5°N and the Antarctic Circumpolar Current (ACC) transport were shown to respectively vary by about ~23% (1 σ) and 28% around the ensemble-mean value [*Danabasoglu et al.*, 2014; *Farneti et al.*, 2015; *Danabasoglu et al.*, 2016]. In similar vein, the goal of the Flux-Anomaly-Forced Model Intercomparison Project (FAFMIP) is to quantify the spread in simulated OHU and sea level change by running different coupled climate models with a fixed set of air-sea fluxes under climate change [*Gregory et al.*, 2016]. In contrast, *Bouttes and Gregory* [2014] considered the case for a fixed coupled climate model to quantify the role of wind and buoyancy forcing as computed by different CMIP5 models in setting the spatial patterns of sea level rise under a transient 1% CO_2 climate change scenario.

A comprehensive framework to compare the two major sources of uncertainties in ocean circulation and heat uptake in climate models — uncertainties in air-sea fluxes on one hand and uncertainties in model parameters such as vertical diffusion on the other hand — is still missing and will be introduced here. Section 2 describes the model setup in which an ocean-only model (MITgcm) is spun-up with the momentum and buoyancy fluxes of 28 models participating in CMIP5. We refer to this model set as "CMIP5 climate models" in the following for brevity. The model's vertical diffusivity and mesoscale eddy-related thickness diffusion are sampled in two smaller ensembles, where a single set of air-sea fluxes is used. Section 3 presents the steady state meridional overturning circulations (MOC) in the ocean-only ensemble and shows the contribution of the different sources of uncertainty to the change in both key circulation metrics and heat content under climate change. A discussion and conclusions are presented in section 4.

2. Climate Models and Forcing Data

2.1. MITgcm Ocean Model

We use the MITgcm primitive equation ocean model [*Marshall et al.*, 1997], henceforth referred to as the ocean model. The resolution is relatively coarse to allow for a large number of numerical simulations and extensive sensitivity studies at low computational cost. The model setup has realistic bathymetry, a regular horizontal 2.8° × 2.8° longitude × latitude grid with 15 irregular-spaced vertical levels. The vertical diffusivity coefficient (κ_v) is a function of depth [*Bryan and Lewis*, 1979] with a default profile ranging from $k_v^s = 3 \times 10^{-5}$ m^2/s at the surface to $k_v^b = 18 \times 10^{-5}$ m^2/s near the bottom. The model features an implicit free surface and uses a convective adjustment scheme. Geostrophic mesoscale eddies are represented by a skew flux implementation of the *Gent and McWilliams* [1990] eddy parameterization scheme with a default thickness diffusion coefficient $\kappa_{GM} = 1000$ m^2/s.

The momentum and buoyancy boundary conditions at the sea surface are given by

$$\mathcal{F}_u = \frac{\tau_x}{\rho_0 \Delta z_s} \tag{1}$$

$$\mathcal{F}_v = \frac{\tau_y}{\rho_0 \Delta z_s} \tag{2}$$

$$\mathcal{F}_\theta = -\lambda_\theta(\mathrm{SST} - \theta^*) - \frac{1}{\rho_0 c_p \Delta z_s} Q \tag{3}$$

$$\mathcal{F}_S = -\lambda_S(\mathrm{SSS} - S^*) + \frac{S_0}{\Delta z_s}(E - P)\,. \tag{4}$$

The model is forced with an annual cycle of prescribed monthly mean momentum fluxes by zonal and meridional winds (τ_x and τ_y, respectively), net surface heat fluxes Q (the sum of net longwave, net shortwave radiation, sensible and latent heat fluxes) and freshwater fluxes $E - P$ as the residual of evaporation and precipitation (neglecting runoff). The sign of heat and freshwater fluxes are defined such that heat (freshwater) from the ocean to the atmosphere are positive. To enable a quasi steady state, the model's sea surface temperature (SST) and salinity (SSS) values are restored to specified restoring values (θ^* and S^*, respectively) with commonly employed restoring timescales of 2 months for temperature (λ_θ) and 3 months for salinity (λ_S), resulting in mixed boundary conditions discussed in *Haney* [1971]. The corresponding piston velocities are 0.83 m/d for the temperature restoring term and 0.55 m/d for salinity, respectively. The constants ρ_0, S_0, and c_p denote a reference density, salinity, and the heat capacity of seawater, respectively, and Δz_s is the thickness of the model's surface layer. The surface boundary conditions will be taken from reanalysis and state-of-the-art climate simulations as explained in the following subsections.

2.2. CMIP5 Data

We use monthly mean climate model output from the Coupled Model Intercomparison Project Phase 5 (CMIP5) ensemble from two scenarios: the preindustrial control simulations (`piControl`) and a transient climate change scenario in which the atmospheric carbon dioxide (CO_2) concentration is increased by 1% each year (1% CO_2) [*Taylor et al.*, 2012]. In total, we use the simulated surface fields from 28 CMIP5 climate models listed in Table S1 of the supporting information. We compute the monthly mean climatologies for the set of surface variables (SST, SSS, Q, $E - P$, τ_x, and τ_y) for each month of the year based on the first 250 years of each

preindustrial control simulations. The surface forcing from the 1% CO2 scenario is described in section 2.4. All surface fields were interpolated to the regular horizontal 2.8° × 2.8° longitude × latitude grid of the MITgcm ocean model. Errors in surface fluxes are present due to the nonconservative nature of the interpolation used. We further use the potential temperature and salinity fields as well as zonally averaged meridional stream functions where available (see supporting information) for diagnostic purposes.

2.3. Reanalysis Products

We further consider air-sea fluxes from different observation-based products. We use two reanalysis products: the *MERRA* Reanalysis (NASA's Modern Era Retrospective-Analysis for Research and Applications) [*Rienecker et al.*, 2011] and the *ERA-Interim* Reanalysis [*Dee et al.*, 2011]. We use the monthly mean fields during the period 1979–2014 to compute monthly climatologies for the buoyancy and wind forcing fields. We also use the Surface Flux Data Set of the UK's National Oceanography Centre (*NOC*) whose air-sea fluxes are derived from observed and bias-corrected surface meteorological parameters using bulk parameterizations [*Berry and Kent*, 2011]. Additionally, we use a standard surface flux product from the MITgcm repository based on a climatological annual cycle (*Trenberth et al.* [1989] and *Jiang et al.* [1999], referred to as *BLEND*). The surface flux fields of these four data sets were interpolated onto the MITgcm grid as well.

2.4. Experiment Design

We use the monthly mean climatological surface wind stress fields, heat, and freshwater fluxes from the 28 CMIP5 models and the four observation-based products in the momentum and buoyancy boundary conditions of the MITgcm (equations (1)–(4)), resulting in a 32-member ensemble. For the CMIP5-driven ensemble members, the monthly mean climatological simulated SST and SSS fields of each model are used as restoring temperature (θ^*) and salinity (S^*) data in order to reproduce the sea surface properties of each CMIP5 model as closely as possible. For consistency, we use the CMIP5 ensemble-mean SST and SSS values as restoring fields for the case of the four observation-based products. Each ensemble member was spun-up for 1000 years and the values presented in this paper are time averages of an additional 90 years of simulation (i.e., years 1000–1090).

To compare the spread in ocean circulation indices due to different air-sea fluxes in the 32-member ensemble with the spread associated with choices of the physical parameters related to vertical diffusion (κ_v) and unresolved mesoscale eddy effects (κ_{GM}), we further run two smaller MITgcm ensembles in which we vary the two parameters individually as illustrated in Figure S1 in the supporting information. In those simulations, we use the CMIP5 ensemble-mean values of the surface fields (SST, SSS, Q, $E-P$, τ_x, and τ_y) to sample only the parameter uncertainty associated with κ_v and κ_{GM}. The value of the surface diffusivity κ_v^s ranges from 0.1 to 1 cm^2/s and the entire depth profile is increased by increments of $\delta\kappa_v = 0.1$ cm^2/s. The value of the thickness diffusion parameter κ_{GM} ranges from 0 to 1600 m^2/s in a nine-member ensemble which roughly approximates the range of κ_{GM} values in CMIP5 (Figure S1). All ensemble members were spun-up for 1000 years.

After the spin-up period, we further run the ensemble for another 90 years in which the monthly air-sea fluxes and monthly sea surface properties from the transient climate change scenario (1% CO_2) are used to drive the MITgcm (data from 23 out of 28 CMIP5 models was used). For the two smaller ensembles in which the model parameters κ_v and κ_{GM} are varied, we use the CMIP5 ensemble mean of the air-sea fluxes, SST and SSS values. To minimize the impact of the surface-restoring terms during the warming scenario, we filtered the monthly forcing sets using a decadal running mean. All results presented for the transient climate change scenario are calculated at the time of CO_2 doubling.

3. Results

3.1. Uncertainty From Air-Sea Fluxes

We start by revisiting the spread in air-sea fluxes and variables in the CMIP5 ensemble and observation-based products. In Figure 1, we compare the CMIP5 ensemble spread to the ensemble mean.

The CMIP5 ensemble reproduces broadly the zonally averaged features of SST and SSS patterns of the *World Ocean Atlas 2009* [*Locarnini et al.*, 2010; *Antonov et al.*, 2010] (Figures 1a, 1b). However, the models are generally too salty in the Northern Hemisphere subpolar latitudes, possibly due to the summer bias of observations. The ensemble spread compared to the ensemble mean is small for SSS (1–3%). In terms of SST, the spread strongly increases poleward, reaching up to ~25% of the mean SST (note that a change of units to Kelvin will change the number, but the spread at high latitudes in SST is still larger than that at low latitudes). The spread in sea surface density values is shown in the supporting information.

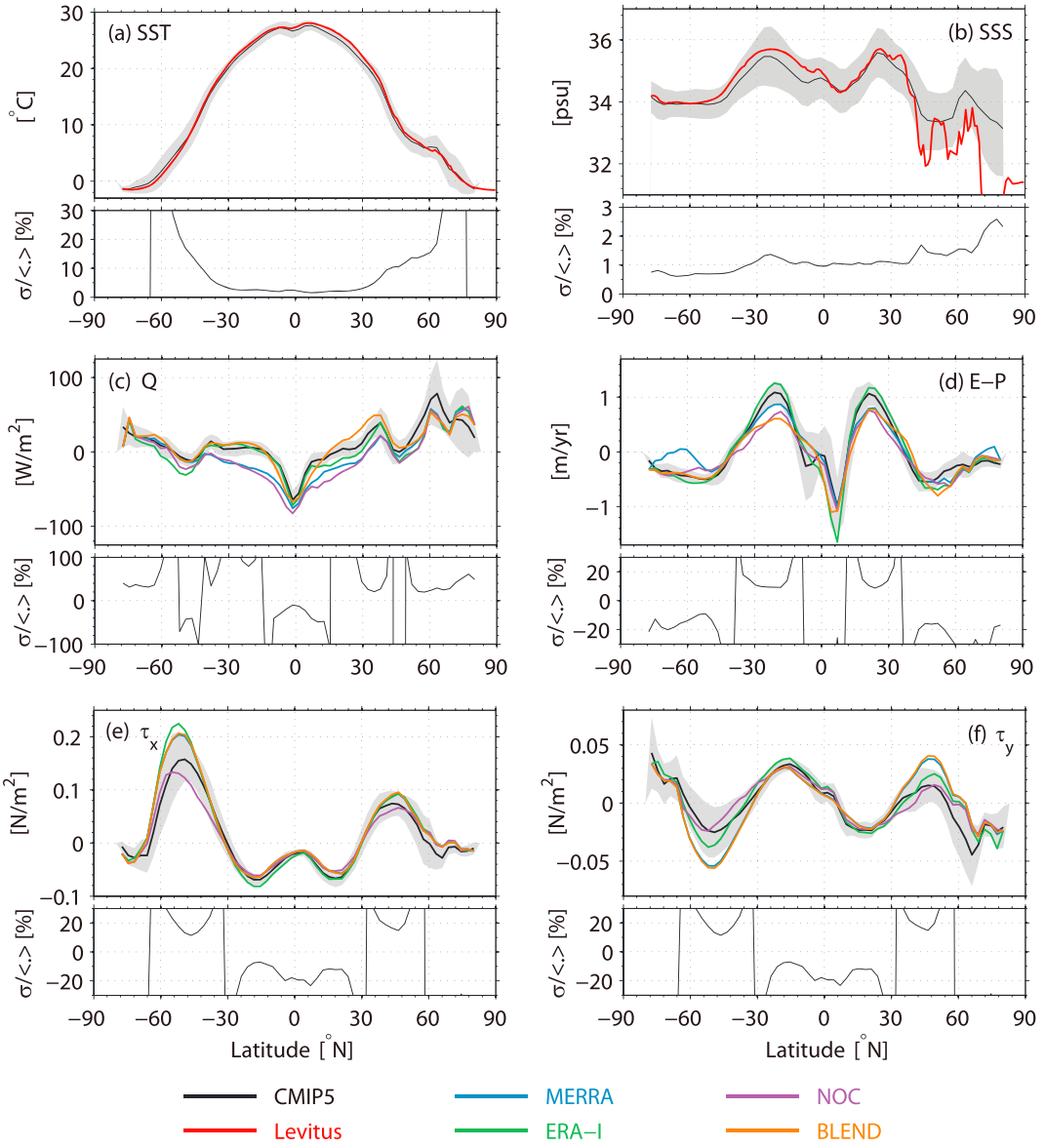

Figure 1. CMIP5 preindustrial control simulations (solid black lines indicate the ensemble mean and grey shadings show the two standard deviations around the mean) for zonally averaged: (a) sea surface temperatures (*SST*); (b) sea surface salinities (*SSS*); (c) net surface heat fluxes, where positive fluxes are directed from the ocean to the atmosphere (*Q*); (d) freshwater fluxes where a positive value indicates a net salt flux into the ocean (*E-P*); (e) zonal wind stress (τ_x), and (f) meridional wind stress (τ_y). The bottom panels indicate the ratio (in percent) of ensemble-spread to ensemble-mean values. For comparison, observed climatological SST and SSS from *The World Ocean Atlas 2009* [*Locarnini et al.*, 2010; *Antonov et al.*, 2010] and estimates of air-sea fluxes from four reanalysis products (MERRA, NOC, ERA-I, and BLEND, see section 2) are shown in colored lines.

Figures 1c and 1d indicate that there are significant uncertainties in the net heat and freshwater fluxes both in the coupled models and in the reanalysis products. While the CMIP5 models compare well with the reanalyses at the equator, they strongly underestimate the heat flux between 30°S and 30°N where the intermodel spread can be as large as the mean energy input. In the Northern Hemisphere subpolar latitudes, the spread in heat fluxes is extremely large, ranging between 40 and 120 W/m^2, far larger than observationally based estimates. The coupled models overestimate the evaporation in the subtropical gyres. Additionally, the freshening of the Northern Hemisphere subpolar latitudes is underestimated in the models compared to the reanalyses. The spread in zonal and meridional wind stress in all data sets are dominated by uncertainties in easterly winds in the Extratropics (Figures 1e and 1f). The spread in the maximum zonal wind stress in

the Southern Ocean is about 13% in the CMIP5 ensemble and 21% across the reanalyses. For a complete assessment of the CMIP5 biases and spread, the reader is referred to *Flato et al.* [2013].

By construction, the forcing fields of the MITgcm ensemble, given by (1)–(4), closely match the CMIP5 ensemble (see Figures S5 and S6). However, it is clear that the spread in CMIP5 and MITgcm air-sea fluxes is often larger than the spread in observational product (Figure 1) with serious implications for simulating the ocean circulation as discussed below.

3.2. Ocean Circulation

Figure 2 compares the zonally averaged stream functions in the Atlantic Ocean between the CMIP5 models (solid contours; data from 11 models were available) and the corresponding MITgcm ensemble members (filled contours). Using only the surface forcing from the corresponding coupled model as described in section 2, Figure 2a shows that the ocean-only model captures the spatial characteristics of the circulation of the particular CMIP5 model to a large degree. For example, the depth and meridional profile of the streamline separating the upper and abyssal cell are very similar in the fully coupled and the ocean-only ensemble. The location of the maximum of the overturning stream function at middepth is slightly farther north in the MITgcm ensemble compared to the CMIP5 ensemble, which is likely related to the geometry and bathymetry of the model.

Figure 2b compares the maximum Atlantic Meridional Overturning Circulation (AMOC) values, ψ_{AMOC}, from the MITgcm ensemble with the corresponding values from the historical CMIP5 model simulations ([*Wang et al.*, 2014], data from 14 out of 28 ensemble members were available). The index ψ_{AMOC} is defined as the maximum stream function in the Atlantic between 20°N and 60°N and below 500 m. The mean AMOC strength in the two ensembles are strongly correlated, $r = 0.9$, and the spread in AMOC in the MITgcm ensemble forced with air-sea fluxes matches the spread in the CMIP5 ensemble. Both the lowest and highest AMOC values (models 21 and 27) in the CMIP5 ensemble correspond to the weakest and strongest AMOC values in the ocean-only ensemble, respectively. Removing these extreme values still results in strong correlations: $r = 0.83$ without model 21, $r = 0.89$ without model 27, or $r = 0.78$ when both models are removed. The AMOC in the MITgcm ensemble underestimates the underlying CMIP5 overturning strength on average by 25%, with an ensemble mean of 14.8 Sv versus 20.6 Sv. Figure 2c compares the volume transport of the ACC at Drake Passage at 68°W, estimated by the maximum barotropic stream function and denoted by ψ_{ACC}, of the MITgcm ensemble with the corresponding values from the historical CMIP5 model simulations ([*Meijers et al.*, 2012], again 14 out of 28 ensemble members). The ACC strength in the two ensembles are positively correlated ($r = 0.6$). However, the ACC transport in the MITgcm ensemble is strongly underestimating the underlying CMIP5 volume transports on average by about 50% (68.4 Sv versus 140.9 Sv). For the ACC strength, the spread in the CMIP5 (80–240 Sv) is much larger than the spread in the MITgcm ensemble (44–96 Sv), yet the ocean-only spread is substantial. The weaker AMOC and ACC strengths in the ocean-only setup are potentially due to a combination of the coarse resolution of the MITgcm, the choice of model parameters, and missing air-sea feedbacks. The circulation indices of each model are tabulated in the supporting information. Note that we only used CMIP5 historical values, rather than control values as those were not available. Therefore, the biases in transport might be related to the lack of historical forcing in the MITgcm simulations.

We continue to examine how the intermodel differences in surface variables impact the strength and spatial characteristics of the ocean circulation. The global residual MOC (Eulerian plus eddy parameterized) of the MITgcm ocean-only ensemble is shown in Figure 3. The 32 MOCs shown in Figure 3 differ only in their SST and SSS restoring profiles and wind and buoyancy fluxes, while the model parameters (i.e., κ_v and κ_{GM}) are the same for each ensemble member.

The ensemble features a wide range of circulations both in terms of overall magnitude and spatial structure of the two overturning cells. The upper cell is associated with sinking of dense water in the high-latitude Atlantic that partly upwells at low latitudes via diapycnal mixing and partly in the Southern Ocean due to Ekman suction. The abyssal cell is associated with the formation of Antarctic Bottom Water (AABW). For example, the MOC simulated using the air-sea fluxes from the Institut Pierre Simon Laplace climate models have generally a weak upper cell accompanied by a strong abyssal cell (models 19, 20, and 21). In contrast, the two model versions from the NorESM (models 27 and 28) feature a vigorous upper cell (in the North Atlantic), which penetrates to 3000 m depth with only a weak abyssal cell. The range of circulations can be for the most part attributed to discrepancies in high-latitude forcing (see Figure S9). Simulations with a strong heat loss in the

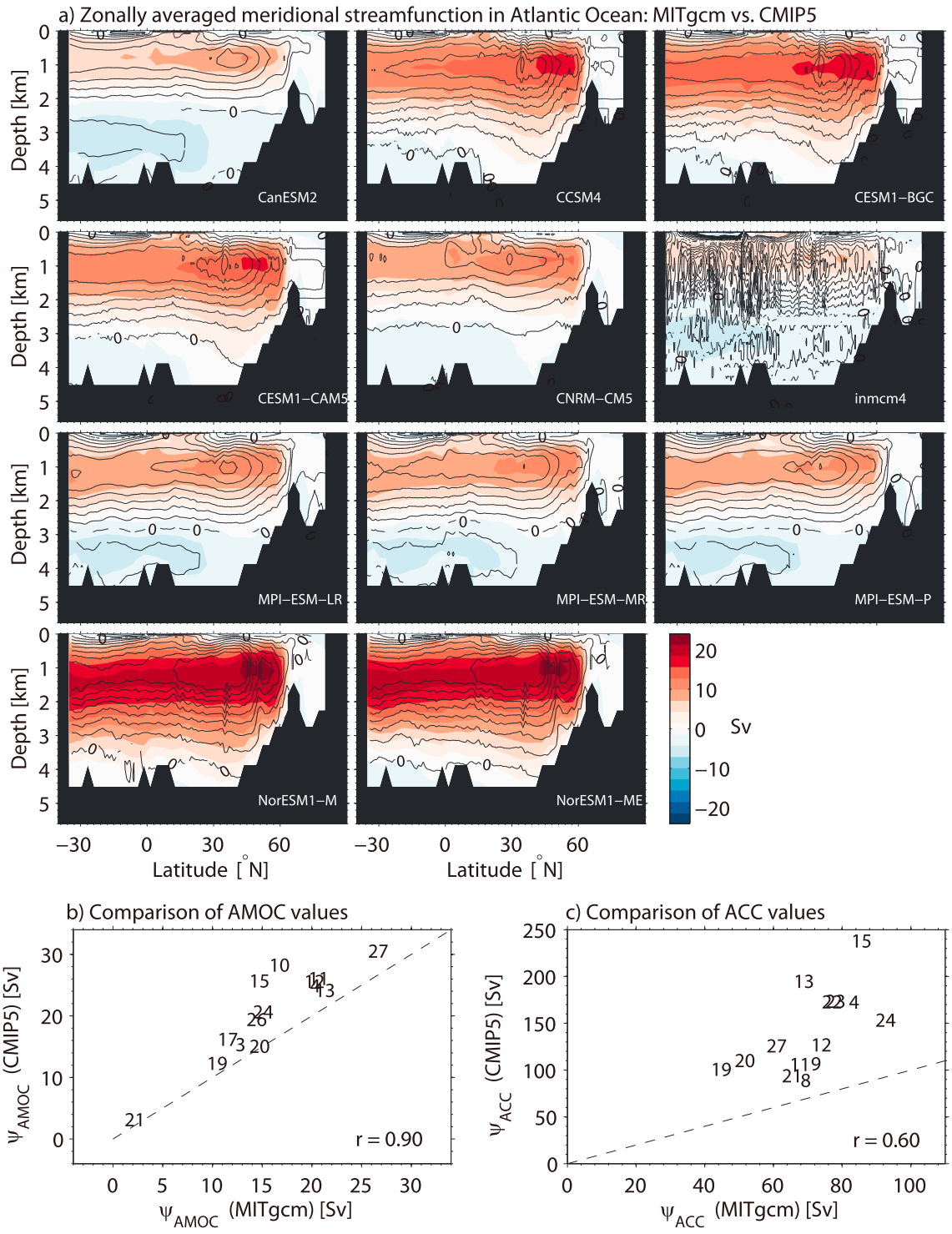

Figure 2. (a) Zonally averaged Eulerian stream functions in the Atlantic Ocean for 11 CMIP5 models (solid contours with a spacing of 3 Sv) and the corresponding MITgcm ensemble members (filled contours). Units are in Sverdrups (1 Sv = 10^6 m^3 s^{-1}]. (b) Maximum Atlantic Meridional Overturning Circulation (ψ_{AMOC}), and (c) Drake Passage Transport (ψ_{ACC}) comparison in the MITgcm ensemble with the corresponding CMIP5 values of the historical simulations [*Wang et al.*, 2014; *Meijers et al.*, 2012]. Correlation coefficients *r* are given in each panel.

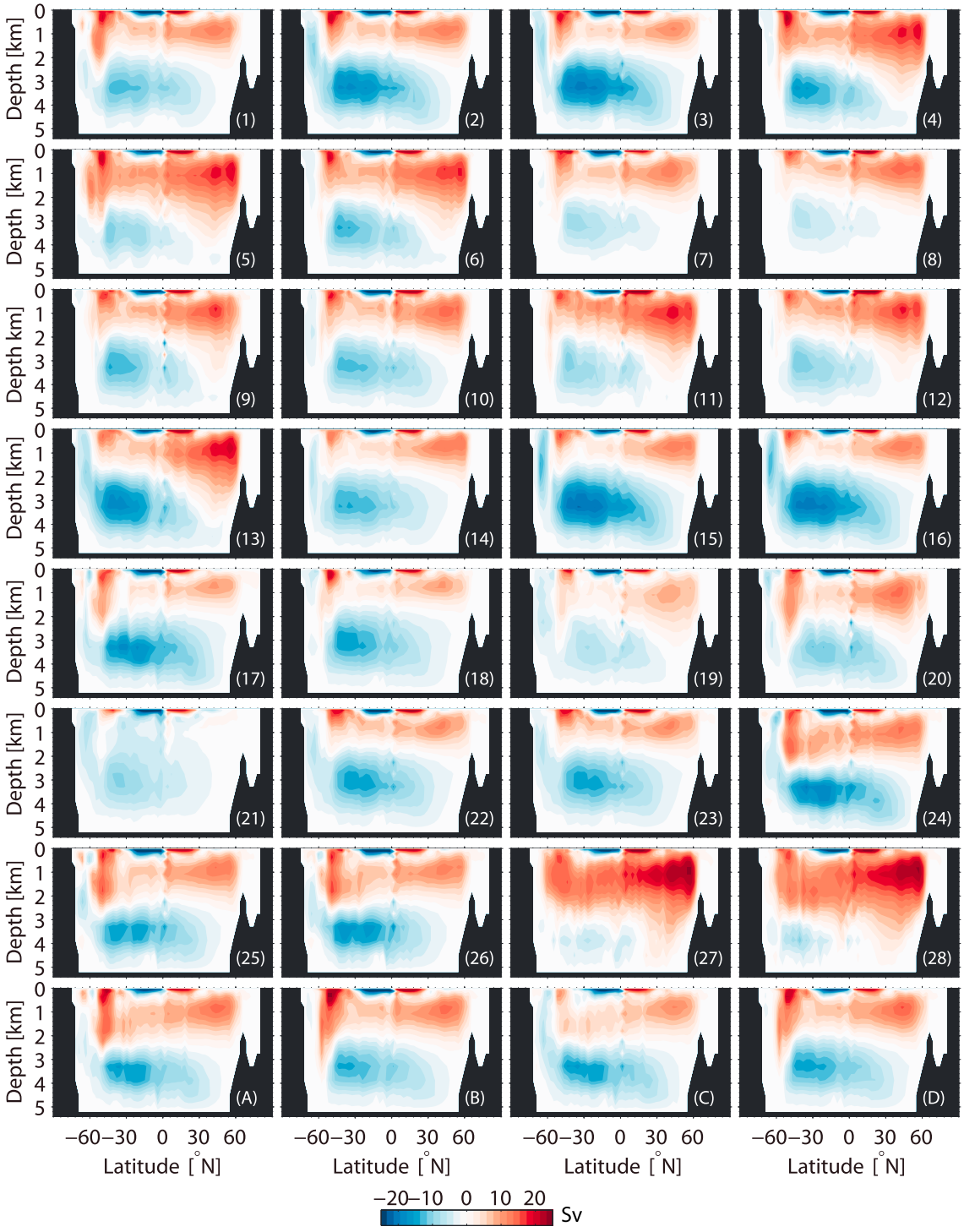

Figure 3. Zonally averaged residual (Eulerian and eddy parameterized) stream functions (units in Sv) of the MITgcm ocean model forced by (1–28) CMIP5 air-sea fluxes and (a–d) four reanalysis products.

subpolar region lead to a strong AMOC and upper cell (e.g., model 27). In the upper 2 km in the Southern Ocean, the circulation is determined by the strength and position of the maximum wind stress (Figure S9). The abyssal cell appears to be anticorrelated with the upper cell (i.e., the AMOC strength, not shown) similar to CMIP5 [*Wang et al.*, 2014], and influenced by the restoring of salinity at the southern edge of the domain corresponding to sea ice forcing in MITgcm. The ACC and Southern Ocean residual circulation strength and spread are well correlated; however, the ACC and AMOC are not correlated in either ensemble (not shown).

To first order, we find that the largest spread in the overturning circulation of the ocean-only ensemble is related to the air-sea fluxes, with differences across model versions of a particular institution being only of secondary importance. For example, the overturning circulations derived from the Australian Community Climate and Earth System Simulator (ACCESS) in the top left corner are clearly distinguishable from the overturning features that result from the air-sea fluxes computed by the Norwegian Earth System Models, whereas differences across the individual model versions ACCESS1-0 and ACCESS1-3 (NorESM-M and NorESM-ME, respectively) that are related to different initial condition, resolution, or perturbations in parameters, are much smaller. Figures 3a–3d further indicate that the differences in the four MOCs derived from reanalysis products are qualitatively of similar order of magnitude for the Northern Hemisphere upper cell, with some discrepancies in the Southern Ocean and the abyssal cell.

3.3. Control Versus Climate Change: Role of Air-Sea Fluxes and Model Parameters

We now compare the relative impact of air-sea flux biases and model parameter uncertainties on the spread of AMOC and ACC strength (ψ_{AMOC} and ψ_{ACC}) in the MITgcm ensemble under a steady state climate as well as a transient climate change scenario. Figures 4a–4d display the spread of AMOC and ACC for the following ensembles: the model parameters are fixed and only the momentum and buoyancy fluxes vary (black bars); the CMIP5 ensemble-mean air-sea fluxes are used to drive the ocean model, but either the vertical diffusivity (κ_v; red circles) or the eddy-thickness diffusion coefficient (κ_{GM}; green dots) is varied.

In steady state (Figure 4a), the impact of uncertainties in air-sea fluxes on the AMOC spread is about twice as large as the spread due to individual physical parameter perturbations. The two parameter perturbation ensembles span a similar range of roughly 10 Sv, equivalent to only one standard deviation in the spread due to air-sea fluxes. Our choice of parameter sampling in κ_v and κ_{GM} is limited by numerical stability, but spans a full order of magnitude in the abyssal vertical diffusion/mixing as well as a range nearly as large as the CMIP5 values for the thickness diffusion parameter κ_{GM} (Figure S1). The spread due to air-sea fluxes could be almost matched by model parameter spread if and only if a model does not possess a GM parameterization and has a very high vertical diffusivity (see Figure S10 and section 4).

When the MITgcm model is forced with the simulated air-sea fluxes of the 1% CO_2 scenario (Figure 4c), most models show a decrease in the AMOC strength with an average decrease of −1.9 Sv, corresponding to a reduction of −12.6%. The ensemble spread of 1.7 Sv (1 σ) related to different air-sea fluxes during the climate change scenario clearly dominates the overall change in overturning strength, whereas different values for the model parameters (κ_v and κ_{GM}) have only a small impact on the change and spread of the AMOC strength.

In contrast to the AMOC in the MITgcm ensemble, the various air-sea fluxes and model parameters have a similar impact on the spread of the ACC transport (Figures 4b and 4d) for the control and climate change scenarios. The spread due to model parameters could be increased if simulations were run with very high vertical diffusivity and no GM parameterization (see Figure S10). Most ensemble members show a strengthening of the ACC transport under climate change with an average increase of about 6 Sv (corresponding to 8% compared to the steady state transport). In CMIP5, however, the ensemble members do not show a consistent sign in the change of ACC transport under two emission scenarios [*Meijers et al.*, 2012]. The differences between the fully coupled (CMIP5) and ocean-only (MITgcm) ensemble is again likely related to the coarse resolution of the MITgcm configuration used here and the use of restoring terms rather than an interactive air-sea coupling (see section 2).

We conclude this section by considering the zonally integrated and basin-scale OHU in the two ensembles. For fixed model parameters, the MITgcm ensemble driven with the CMIP5 air-sea fluxes reproduces the CMIP5 OHU on average well (Figure 4e), including the maximum heat uptake in the Southern Ocean [e.g., *Frölicher et al.*, 2015]. The largest differences between the two ensembles is related to the spread in the MITgcm being larger than that of CMIP5. The differences are prominent at high latitudes and along western boundary

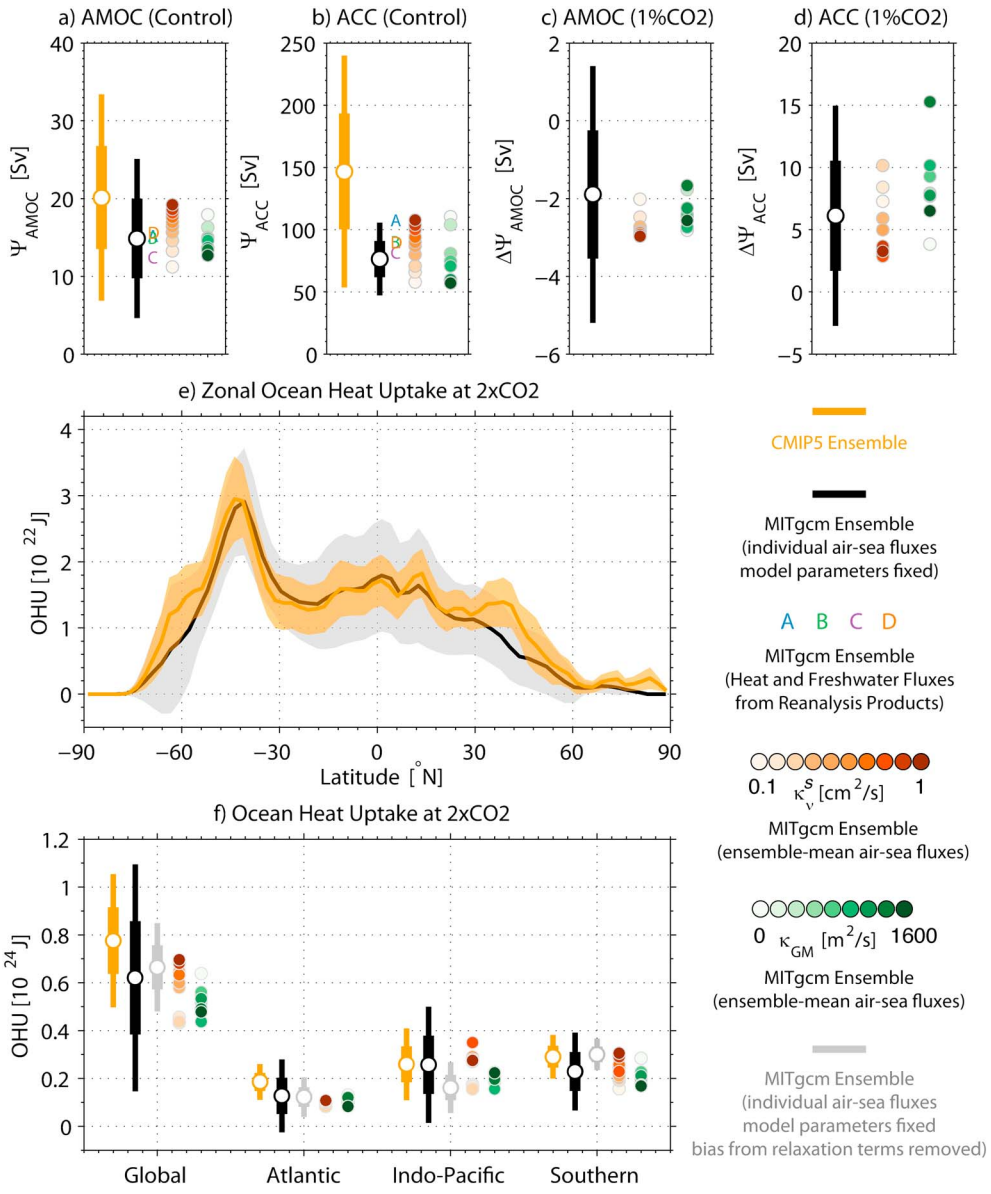

Figure 4. Comparison of different sources of uncertainty on (a) AMOC and (b) ACC values in steady state and (c, d) their change under transient climate change at time of $2xCO_2$. The uncertainty ranges for the CMIP5 models (orange bars) and the MITgcm ensemble with varied air-sea fluxes and fixed model parameters (black bars) denote one and two standard deviations around the ensemble mean. The colored circles refer to the two smaller ensembles in which subgrid parameters are perturbed: eddy thickness diffusion (κ_{GM}, green) and vertical diffusivity (κ_v, red) with the legend indicating the surface value of the coefficient—see section 2. (e) Zonally integrated ocean heat uptake (OHU) at time of $2xCO_2$ for the MITgcm ensemble driven by the different CMIP5 air-sea fluxes (black) and the CMIP5 ensemble (orange). Solid lines indicate the ensemble mean, and the shadings show the ±1 standard deviations around the mean. (f) Basin perspective on the contributions of different sources of uncertainties to OHU (legend as in Figures 4a–4d). Corrected MITgcm ensemble mean and ensemble spread are shown in grey and are a representation of the lower bound influence of air-sea fluxes on the OHU (see text and supporting information for explanation about the restoring term correction). The northern boundary of the Southern Ocean was chosen to be 30°S, whereas the Atlantic and Indo-Pacific Oceans extend to 66°N.

currents, which is likely due to combined and intertwined influence of the mixed boundary conditions, the lack of dynamic sea ice model and the resolution and geometry of the ocean model.

Due to the mixed boundary conditions (equation (3)), the heat balance in MITgcm comprises a term related to the CMIP5-derived heat fluxes (Q) and a contribution from the imbalance between simulated and restoring values in sea surface temperatures ($-\lambda_\theta(\mathrm{SST}-\theta^*)$). Using MITgcm diagnostics for both terms, we can correct for the heat flux uncertainty associated with the restoring terms (see supporting information) to provide a lower bound on the impact of direct air-sea fluxes onto the OHU. Figure 4f shows the spread in global and basin-scale OHU for the CMIP5 (orange), the MITgcm driven by air-sea fluxes (black), and with the corrected ensemble-mean and ensemble-spread values (grey). The Southern Ocean and Indo-Pacific dominate the global heat uptake, followed by the Atlantic in both the MITgcm (corrected or not) and the CMIP5 ensemble. This result is in part determined by the size of the basin rather than due to changes in physical processes (cf. Figure S8 for normalized OHU). The spread in global OHU is equally due to model parameters and air-sea fluxes. Additional simulations with extreme parameter values reaffirm that model parameters are very crucial for global and regional OHU, except in the Atlantic (see Figure S10).

The spread of Atlantic OHU is dominated by the air-sea fluxes. This result is in agreement with the AMOC sensitivity to air-sea fluxes under control and 1% CO_2 scenarios described above and potentially with the role of the AMOC [e.g., *Kostov et al.*, 2014] and associated air-sea feedbacks [e.g., *Gregory et al.*, 2016] in OHU. The spread of OHU in the Pacific is dominated by changes in the vertical diffusion coefficient, due to the strong influence of low-latitude diapycnal mixing and the lack of an overturning circulation. In the Southern Ocean, the heat uptake is mainly attributable to passive Ekman pumping and Southern Ocean stratification. Therefore, it is not surprising that the eddy mixing coefficient is central in the spread of heat uptake due to its role in setting the stratification and its adjustment timescale under climate change [*Marshall and Zanna*, 2014]. The vertical diffusivity coefficient also plays an important role in Southern Ocean heat uptake by modifying the stratification. Interestingly, the spread in the Southern Ocean heat uptake does not correlate with the spread in ACC strength.

4. Discussion and Conclusions

We presented a new modeling framework to quantify the impact of uncertainty in surface forcing and model parameters on the spread in oceanic circulation and OHU. We considered both steady state climate and transient CO_2 radiative forcing simulations. The modeling framework uses the simulated fields of the fully coupled CMIP5 models to drive an ocean-only coarse-resolution climate model. The ocean-only ensemble reproduces the temperature and salinity patterns of the underlying CMIP5 models well (Figures S2 and S3). The main discrepancies among the two ensembles are found in the Western Boundary Currents and the Southern Ocean (see Figure S2) due to the coarse-resolution setup. Our results thus extend and complement previous experiments with ocean-only models to study OHU and circulation changes under climate change [i.e., *Xie and Vallis*, 2012; *Marshall et al.*, 2015] and could be part of the OMIP initiative [*Griffies et al.*, 2016]. For example, *Marshall et al.* [2015] investigate the role of the ocean circulation in OHU under the 4xCO_2 climate change scenario in the MITgcm ocean-only model by using a constant climate feedback parameter. A particular novelty of the approach introduced here is that no assumptions about the spatiotemporal patterns of the fluxes or about the magnitude of the radiative feedback parameter are made. These quantities are implicitly accounted for in the CMIP5 air-sea fluxes and surface properties used to drive the ocean model.

For a steady state climate, we show that the spread in key circulation indices such as the maximum transport of the AMOC and the volume transport of the ACC at Drake Passage can vary by 34% (AMOC) and 19% (ACC) for a given set of physical parameters in the ocean model. Importantly, the spread in the AMOC strength is of similar magnitude as the range of values that results from driving a set of different ocean models with a fixed set of CORE-II atmospheric forcing data [*Danabasoglu et al.*, 2014, 2016]. This result clearly highlights the first-order influence of surface flux biases on the spread in simulated ocean circulations. While the air-sea fluxes corresponding to modern climate conditions are used to spin-up the ocean model, the variety of overturning circulations that result from the range of air-sea fluxes has further implications for simulating past climates. Qualitatively, the steady state MOCs in Figure 3 make the distinction between the modern ocean circulation and the depth and meridional structure of the two overturning cells of past ocean states difficult, i.e., in the Last Glacial Maximum with an extended abyssal cell and a more shallow upper cell [*Ferrari et al.*, 2014; *Watson et al.*, 2015], thus highlighting the need for strong observational constraints for air-sea fluxes to

use in climate models for simulating past, present, and future climates. The air-sea fluxes and model parameters have a similar impact on the spread of the ACC transport for the control and climate change scenarios. The ACC and Southern Ocean circulations are sensitive to factors related to the ocean stratification and its response to forcing.

The modeling framework introduced here further allowed to compare the relative impact of uncertainties in sea surface properties and physical model parameters on the model spread in the AMOC strength. We showed that uncertainty from sea surface forcing is about twice as large as physical model parameter uncertainties (Figure 4). For OHU under transient climate change, we find that the sensitivity to uncertainties at the sea surface or to model parameters differ across the basins. In the Atlantic, the ranges of OHU values are dominated by different air-sea fluxes, while in the Pacific and Southern Ocean, the spread related to the various sources of uncertainty are comparable. We hypothesized, however, that the use of mixed boundary conditions could constitute additional sources and sinks of heat at the surface and at depth, leading to discrepancies between SST and heat uptake in an ocean-only model (see supporting information). The OHU normalized by the size of each basin is shown in Figure S8 for the CMIP5 and the MITgcm ensembles, representing change in temperature each basin will experience. Unlike in the past 50 years, the temperature change under future transient climate change in the CMIP5 ensemble is dominated by changes in the Atlantic rather than by passive advection of heat by the mean circulation in the Southern Ocean. The result is likely associated with changes in the AMOC and deep convection leading to large changes in temperature. The strong temperature change in the Atlantic, compared to other basins, is not well captured by the MITgcm ensemble. Therefore, the role of the AMOC and high-latitudes air-sea fluxes and coupled feedbacks in the Atlantic under climate change are of crucial importance for determining ocean heat storage, and further work is required to understand the physical processes at play.

There are further limitations and caveats in the modeling framework introduced here. In addition to its rather coarse resolution and associated geometry, which clearly constrains the dynamics of ocean circulation, and the use of monthly mean climatological forcings, the MITgcm setup used here does not include a sea ice model or an overflow parameterization [*Yeager and Danabasoglu*, 2012], which could partly explain the high-latitude sea surface biases (Figures S2 and S4) with some impact on the AMOC strength and the formation of AABW. Furthermore, the lack of variability, except for the seasonal cycle, in the surface forcing might be a cause for the discrepancies in large-scale features. However, despite these caveats, the results presented in this study (i.e., Figure 2) suggest that the first-order differences in the ocean circulation in the CMIP5 ensemble can be largely attributed to different air-sea coupling and the associated differences in buoyancy and wind fluxes, and differences across model versions of a particular institution are only of secondary importance, at least for the coarse-resolution framework used here.

Acknowledgments
We thank Kyle Armour and Jonathan Gregory for useful discussions. We acknowledge the World Climate Research Programme's Working Group on Coupled Modelling, which is responsible for CMIP, and we thank the climate modeling groups (listed in Table S1 of the supporting information) for producing and making available their model output. We thank the MITgcm developers as well as Urs Beyerle of the Swiss Federal Institute of Technology in Zurich (ETHZ) for access to their CMIP5 data archive and two reviewers for their useful comments. M.B.H. was supported by the Swiss National Science Foundation grant P300P2_158448. Modeling results presented in this study are available upon request to the corresponding author.

References

Antonov, J. I., D. Seidov, T. P. Boyer, R. A. Locarnini, A. V. Mishonov, H. E. Garcia, O. K. Baranova, M. M. Zweng, and D. R. Johnson (2010), World Ocean Atlas 2009, in *Volume 2: Salinity*, edited by S. Levitus, pp. 184, U.S. Gov. Print. Off., Washington, D. C.

Berry, D. I., and E. C. Kent (2011), Air–Sea fluxes from ICOADS: The construction of a new gridded dataset with uncertainty estimates, *Int. J. Climatol.*, *31*(7), 987–1001.

Bouttes, N., and J. Gregory (2014), Attribution of the spatial pattern of CO_2-forced sea level change to ocean surface flux changes, *Environ. Res. Lett.*, *9*(3), 034004.

Bryan, K., and L. Lewis (1979), A water mass model of the world ocean, *J. Geophys. Res.*, *84*(C5), 2503–2517.

Danabasoglu, G., et al. (2014), North Atlantic simulations in coordinated ocean-ice reference experiments phase II (CORE-II). Part I: Mean states, *Ocean Modell.*, *73*, 76–107.

Danabasoglu, G., et al. (2016), North Atlantic simulations in Coordinated Ocean-ice Reference Experiments phase II (CORE-II). Part II: Inter-annual to decadal variability, *Ocean Modell.*, *97*, 65–90.

Dee, D., et al. (2011), The ERA-Interim reanalysis: Configuration and performance of the data assimilation system, *Q. J. R. Meteorol. Soc.*, *137*(656), 553–597.

Farneti, R., et al. (2015), An assessment of Antarctic Circumpolar Current and Southern Ocean meridional overturning circulation during 1958–2007 in a suite of interannual CORE-II simulations, *Ocean Modell.*, *93*, 84–120.

Ferrari, R., and C. Wunsch (2008), Ocean circulation kinetic energy: Reservoirs, sources, and sinks, *Annu. Revi. Fluid Mech.*, *41*(1), 253–282.

Ferrari, R., M. F. Jansen, J. F. Adkins, A. Burke, A. L. Stewart, and A. F. Thompson (2014), Antarctic sea ice control on ocean circulation in present and glacial climates, *Proc. Natl. Acad. Sci. U.S.A.*, *111*(24), 8753–8758.

Flato, G., et al. (2013), Evaluation of climate models, in *The Physical Science Basis. Contribution of Working Group I to the Fifth Assessment Report of the Intergovernmental Panel on Climate Change*, edited by T. Stocker et al., pp. 741–866 Cambridge Univ. Press, Cambridge, U. K., and New York.

Frölicher, T. L., J. L. Sarmiento, D. J. Paynter, J. P. Dunne, J. P. Krasting, and M. Winton (2015), Dominance of the Southern Ocean in anthropogenic carbon and heat uptake in CMIP5 models, *J. Clim.*, *28*(2), 862–886.

Gent, P. R., and J. C. McWilliams (1990), Isopycnal mixing in ocean circulation models, *J. Phys. Oceanogr.*, *20*(1), 150–155.

Gregory, J. M., et al. (2016), The Flux-Anomaly-Forced Model Intercomparison Project (FAFMIP) contribution to CMIP6: Investigation of sea-level and ocean climate change in response to CO_2 forcing, *Geosci. Model Dev. Discuss.*, *2016*, 1–37.

Griffies, S. M., et al. (2016), OMIP contribution to CMIP6: Experimental and diagnostic protocol for the physical component of the Ocean Model Intercomparison Project, *Geosci. Model Dev.*, *9*(9), 3231–3296.

Haney, R. L. (1971), Surface thermal boundary condition for ocean circulation models, *J. Phys. Oceanogr.*, *1*(4), 241–248.

Jiang, S., P. H. Stone, and P. Malanotte-Rizzoli (1999), An assessment of the geophysical fluid dynamics laboratory ocean model with coarse resolution: Annual-mean climatology, *J. Geophys. Res.*, *104*(C11), 25,623–25,645.

Kostov, Y., K. C. Armour, and J. Marshall (2014), Impact of the Atlantic meridional overturning circulation on ocean heat storage and transient climate change, *Geophys. Res. Lett.*, *41*, 2108–2116, doi:10.1002/2013GL058998.

Locarnini, R. A., A. V. Mishonov, J. I. Antonov, T. P. Boyer, H. E. Garcia, O. K. Baranova, M. M. Zweng, and D. R. Johnson (2010), World Ocean Atlas 2009, in *Volume 1: Temperature*, edited by S. Levitus, pp. 184, U.S. Gov. Print. Off., Washington, D. C.

Loeb, N. G., J. M. Lyman, G. C. Johnson, R. P. Allan, D. R. Doelling, T. Wong, B. J. Soden, and G. L. Stephens (2012), Observed changes in top-of-the-atmosphere radiation and upper-ocean heating consistent within uncertainty, *Nat. Geosci.*, *5*(2), 110–113.

Marshall, D. P., and L. Zanna (2014), A conceptual model of ocean heat uptake under climate change, *J. Clim.*, *27*(22), 8444–8465.

Marshall, J., A. Adcroft, C. Hill, L. Perelman, and C. Heisey (1997), A finite-volume, incompressible Navier Stokes model for studies of the ocean on parallel computers, *J. Geophys. Res.*, *102*(C3), 5753–5766.

Marshall, J., J. R. Scott, K. C. Armour, J.-M. Campin, M. Kelley, and A. Romanou (2015), The ocean's role in the transient response of climate to abrupt greenhouse gas forcing, *Clim. Dyn.*, *44*(7–8), 2287–2299.

Meijers, A., E. Shuckburgh, N. Bruneau, J.-B. Sallee, T. Bracegirdle, and Z. Wang (2012), Representation of the Antarctic Circumpolar Current in the CMIP5 climate models and future changes under warming scenarios, *J. Geophys. Res.*, *117*, C12008, doi:10.1029/2012JC008412.

Rienecker, M. M., et al. (2011), MERRA: NASA's modern-era retrospective analysis for research and applications, *J. Clim.*, *24*(14), 3624–3648.

Taylor, K. E., R. J. Stouffer, and G. A. Meehl (2012), An overview of CMIP5 and the experiment design, *Bull. Am. Meteorol. Soc.*, *93*(4), 485–498.

Trenberth, K., J. Olson, and W. Large, (1989), A global wind stress climatology based on ECMWF analyses, Tech. Rep. NCAR/TN-338+STR, NCAR, Boulder, Colo.

Trenberth, K. E., J. M. Caron, and D. P. Stepaniak (2001), The atmospheric energy budget and implications for surface fluxes and ocean heat transports, *Clim. Dyn.*, *17*(4), 259–276.

Valdivieso, M., et al. (2015), An assessment of air–sea heat fluxes from ocean and coupled reanalyses, *Clim. Dyn.*, doi:10.1007/s00382-015-2843-3.

Walin, G. (1982), On the relation between sea-surface heat flow and thermal circulation in the ocean, *Tellus*, *34*(2), 187–195.

Wang, C., L. Zhang, S.-K. Lee, L. Wu, and C. R. Mechoso (2014), A global perspective on CMIP5 climate model biases, *Nat. Clim. Change*, *4*(3), 201–205.

Watson, A. J., G. K. Vallis, and M. Nikurashin (2015), Southern Ocean buoyancy forcing of ocean ventilation and glacial atmospheric CO_2, *Nat. Geosci.*, *8*, 861–864, doi:10.1038/NGEO2538.

Wild, M., D. Folini, M. Z. Hakuba, C. Schär, S. I. Seneviratne, S. Kato, D. Rutan, C. Ammann, E. F. Wood, and G. König-Langlo (2015), The energy balance over land and oceans: An assessment based on direct observations and CMIP5 climate models, *Clim. Dyn.*, *44*(11–12), 3393–3429.

Xie, P., and G. K. Vallis (2012), The passive and active nature of ocean heat uptake in idealized climate change experiments, *Clim. Dyn.*, *38*(3–4), 667–684.

Yeager, S., and G. Danabasoglu (2012), Sensitivity of Atlantic meridional overturning circulation variability to parameterized Nordic Sea overflows in CCSM4, *J. Clim.*, *25*(6), 2077–2103.

Supporting Information for "Drivers of uncertainty in simulated ocean circulation and heat uptake"

M. B. Huber[1] and L. Zanna[1]

Contents of this file

• Section 1 describes the computation of ocean heat uptake in the CMIP5 and MITgcm ensembles.

• Section 2 introduces the method to remove biases in ocean heat uptake associated with the use of mixed boundary conditions in the MITgcm setup.

• Table 1 lists the identifiers for the CMIP5 models used to drive the MITgcm ocean model. It also lists the strength of the Atlantic Meridional Overturning Circulation (AMOC) and the volume transport of the Antarctic Circumpolar Current (ACC) at Drake passage both for the steady-state and the change under a transient climate change simu-

---

Corresponding author: L. Zanna, Department of Physics, University of Oxford, Clarendon Laboratory, Parks Road, Oxford, OX1 3PU, United Kingdom

[1]Department of Physics, University of Oxford, Oxford, United Kingdom

lation (1%CO_2).

• Figure 1 illustrates the parameter sampling of vertical diffusivity (κ_ν) and eddy-related thickness diffusion (κ_{GM}) in the MITgcm ocean model.

• Figure 2 compares biases in sea-surface temperature (SST) and sea-surface salinity (SSS) biases between the MITgcm-ensemble, the CMIP5 coupled models and the observations.

• Figure 3 compares the depth-profiles of potential temperature and salinity for the MITgcm-ensemble, the CMIP5 climate models and the observed climatological profiles.

• Figure 4 illustrates the relative contribution of the relaxation terms on the one hand and of heat and freshwater fluxes on the other hand in the boundary conditions for sea-surface temperature and sea-surface salinity (refer Eqns. 3-4 in the manuscript).

• Figure 5 illustrates the change in sea-surface properties and air-sea fluxes under the transient 1%CO_2 scenario in the CMIP5 ensemble used to drive the MITgcm ocean model.

• Figure 6 shows the equivalent quantities as Fig. 5, but for the MITgcm ensemble. Note that in the bottom panel, the effective fluxes are shown, which are the sum of the relaxation terms and the actual heat and freshwater fluxes that are derived from the CMIP5 ensemble.

• Figure 7 shows the cumulative energy change during the transient 1%CO_2 simulation in the MITgcm ensemble due to contributions from the relaxation term ($-\lambda_\theta(SST-\theta^*)$), CMIP5-derived heat fluxes (Q) and the sum of the two contributions.

• Figure 8 displays the volume-averaged temperature change in individual basins under the transient 1%CO_2 scenario. Note that the Southern Ocean extends here to 30°S, the Atlantic Ocean includes the sector between 30°S–66°N, and the Indian and Pacific Ocean are combined here using the same latitudes range.

• Figure 9 further identifies possible drivers of the spread in the MITgcm ensemble by relating the air-sea fluxes with the overturning circulations using four illustrative ensemble members.

• Figure 10 examines the effect of combining the minimum and maximum values of the two model parameters κ_ν and κ_{GM} on the strength and spread of AMOC and ACC as well as on the magnitude of ocean heat uptake in the MITgcm ensemble.

• Based on the SST and SSS fields of the CMIP5 models depicted in Fig. 1 of the manuscript, Figure 11 shows the corresponding mean and spread across the ensemble for the surface density fields.

1. Computation of ocean heat uptake

For both the CMIP5 and MITgcm ensemble, we consider the global and basin-scale ocean heat content such that

$$OHC(t) = \int_V \rho_0 c_p \theta(t) \mathrm{d}V, \tag{1}$$

where θ is the annually averaged potential temperature at time t, ρ_0=1000 kg/m^3 is the reference density, c_p = 4100 J/(kg·K) is the specific heat of water and $V = A \times H$ is the volume over the corresponding ocean domain A and H is the ocean depth. We define the Southern Ocean domain as extending to 30°S, the Atlantic Ocean includes the sector

between 30°S–66°N, and the Indian and Pacific Ocean are combined here using the same latitudes range.

We define the change of ocean content (OHU) under a transient 1%CO_2 as the difference between the average of the twenty-year period at the end of the simulation (years 60–80) when the atmospheric CO_2 has doubled and the first twenty years, that is:

$$OHU^{1\%CO2} = \overline{OHC^{1\%CO2}}(60-80) - \overline{OHC^{1\%CO2}}(1-20). \quad (2)$$

For the MITgcm ensemble, we also subtract the drift in OHC after the 1,000 year spin-up.

2. Bias correction due to mixed boundary conditions

As mentioned in the manuscript, the MITgcm setup used here employs mixed boundary conditions such that

$$\mathcal{F}_\theta = -\lambda_\theta(SST-\theta^*) - \frac{1}{\rho_0 c_p \Delta z_s} Q \quad (3)$$

$$\mathcal{F}_S = -\lambda_S(SSS-S^*) + \frac{S_0}{\Delta z_s}(E-P), \quad (4)$$

with fixed heat and freshwater fluxes as well as temperature and salinity restoring terms (refer to the manuscript for the detailed description of the variables and constants).

We focus here on the effects that the boundary conditions have on the computation of ocean heat uptake under climate change. From the MITgcm model output, we denote the effective forcing F^{eff} as the sum of the restoring term F_λ and the fixed flux F_Q from Eq. 3 above. These diagnostics have the units W/m^2 - note that the original units of the temperature tendency in Eq. 3 are K/s.

Due to heat conservation, the actual heat input under the climate change simulation over time is given by the area- and time-integrated energy (in Joule) resulting from the

left hand side of Eq. 3, that is:

$$\Delta H = \int_0^t \int_V \mathrm{d}t\mathrm{d}V \rho_0 c_p (\theta(t)^{1\%CO2} - \theta^{control}), \tag{5}$$

where $V = A \times H$ is the ocean volume (e.g, global or basin) with A the surface area of interest (e.g, global or basin) and dt is one year in seconds. Note that for global OHU, we can also write

$$\Delta H = \int_0^t \int_A \mathrm{d}t\mathrm{d}A (F_{eff}^{1\%CO2} - F_{eff}^{control}). \tag{6}$$

The ensemble-mean and ensemble-spread of the heat input for the MITgcm ensemble is shown in Fig. 7 in black for the global ocean and for individual basins. In the absence of restoring terms, or in the case where the MITgcm model is able to evolve perfectly in sync with the CMIP5 sea-surface temperatures, F_λ would be zero. The actual heat uptake would be entirely due to the net heat fluxes (F_Q), which is shown in red in Fig. 7. The contributions resulting from the use of the temperature restoring term is shown in green. Figure 7 shows that on average, the restoring terms contribute little to the ocean heat uptake and that the magnitude of OHU in all basins - except the Pacific Ocean - is small. However, the restoring terms are important when considering the spread of heat input in the MITgcm experiments. We believe that the role of the restoring terms enters due to the diverging behaviour of the MITgcm surface properties compared to that of the CMIP5 models. For example, while the MITgcm is forced by surface fluxes from the CMIP5 models, its SST and SSS might not exactly evolve according to the surface forcing. Therefore, the restoring becomes more prominent, especially in the vicinity of western boundary currents and deep water formation sites near sea-ice. This leads to an altered coupled feedback compared to that of the CMIP5 models. The discrepancies are

likely due to the model resolution and geometry. We thus introduce here a scaling factor for each basin that takes the impact of the restoring terms on the spread of OHU into account, helping us to identify the contribution of the direct heat fluxes forcing on the spread.

Assume that $\mathcal{D}(\mu, \sigma)$ denotes the distribution of ocean heat uptake values of the MITgcm ensemble with ensemble-mean μ and standard deviation σ. Based on the values of Fig. 7, the distributions $\mathcal{D}_{eff}(\mu_{eff}, \sigma_{eff})$, $\mathcal{D}_{\lambda}(\mu_{\lambda}, \sigma_{\lambda})$ and $\mathcal{D}_{\mathcal{Q}}(\mu_{Q}, \sigma_{Q})$ denote the mean and spread of the heat input due to each term in the temperature boundary conditions of the ocean model (Eq. 3). We now define scaling factors $\delta\mu$ and $\delta\sigma$ which quantify the impact of the artificial forcing F_{λ} on the heat uptake for each basin:

$$\delta\mu \quad = \mu_{\lambda} \tag{7}$$

$$\delta\sigma \; = \frac{\sigma_{Q}}{\sigma_{eff}}. \tag{8}$$

Figure 4 of the manuscript shows the distribution $\mathcal{D}(\mu, \sigma)$ as solid black lines around the ensemble-mean. In order to remove the effect of F_{λ} on the ocean heat uptake, we further plot in grey the following distribution: $\mathcal{D}(\mu - \delta\mu, \delta\sigma \cdot \sigma)$. We thus subtract the average effect of the restoring terms on the mean ocean heat uptake distribution in the MITgcm ensemble $(\mu - \delta\mu)$ and also reduce the ensemble-spread by the factor $\delta\sigma$, which ranges between 0.3–0.6 depending on the basin. The scaled ensemble-spread $\delta\sigma \cdot \sigma$ gives thus a more physical interpretation of the impact of uncertainty in surface heat fluxes on ocean heat uptake as the effect of the increase of the ensemble-spread due to the restoring

terms is removed. The corrected spread gives us a lower bound on the role of air-sea fluxes on the spread in the MITgcm ensemble, and therefore in the CMIP5 ensemble.

References

Antonov, J. I., D. Seidov, T. P. Boyer, R. A. Locarnini, A. V. Mishonov, H. E. Garcia, O. K. Baranova, M. M. Zweng, and D. R. Johnson (2010), World Ocean Atlas 2009, in *Volume 2: Salinity*, edited by S. Levitus, p. 184, U.S. Government Printing Office, Washington, D.C.

Bryan, K., and L. Lewis (1979), A water mass model of the world ocean, *Journal of Geophysical Research: Oceans*, *84*(C5), 2503–2517.

Downes, S. M., and A. M. Hogg (2013), Southern Ocean circulation and eddy compensation in CMIP5 models, *Journal of Climate*, *26*(18), 7198–7220.

Locarnini, R. A., A. V. Mishonov, J. I. Antonov, T. P. Boyer, H. E. Garcia, O. K. Baranova, Z. M. M., and D. R. Johnson (2010), World Ocean Atlas 2009, in *Volume 1: Temperature*, edited by S. Levitus, p. 184, U.S. Government Printing Office, Washington, D.C.

Table 1. Model identifiers of CMIP5 climate models (1–28) and four reanalysis datasets (A–D) whose buoyancy and wind forcings are used to drive the MITgcm ocean model (see Section 2). Key circulation indices of the MITgcm-ensemble are given in Sverdrups, 1 Sv = $10^6 m^3/s$. For those model where data was available, the change in AMOC and ACC strength is computed as difference between years 60–80 and 1–20 of the 1%CO_2 scenario.

ID	MODEL	ψ_{AMOC} [Sv]	$\Delta\psi_{AMOC}$ [Sv]	ψ_{ACC} [Sv]	$\Delta\psi_{ACC}$ [Sv]
(1)	ACCESS1-0	13.52	-2.92	79.16	5.88
(2)	ACCESS1-3	14.03	-3.00	99.80	-2.18
(3)	CanESM2	12.31	-0.75	98.34	1.03
(4)	CCSM4	19.79	-2.52	81.98	3.33
(5)	CESM1-BGC	20.46	-2.18	82.24	5.79
(6)	CESM1-CAM5	18.68	x	78.04	x
(7)	CMCC-CM	12.68	x	66.58	x
(8)	CNRM-CM5	- 15.80	-2.82	67.89	12.69
(9)	CSIRO-Mk3-6-0	17.55	-4.32	70.87	5.80
(10)	GFDL-CM3	15.63	-3.79	72.68	5.12
(11)	GFDL-ESM2G	19.55	-3.89	64.68	8.61
(12)	GFDL-ESM2M	19.15	-4.41	70.91	7.46
(13)	GISS-E2-H	20.37	-1.88	65.87	2.46
(14)	GISS-E2-H-CC	13.51	x	82.24	x
(15)	GISS-E2-R	13.72	-1.73	82.65	1.21
(16)	GISS-E2-R-CC	13.24	x	88.80	x
(17)	HadGEM2-ES	10.38	-0.50	93.80	-1.72
(18)	inmcm4	9.36	0.84	100.03	3.46
(19)	IPSL-CM5A-LR	9.32	-0.18	41.78	5.87
(20)	IPSL-CM5A-MR	13.46	-2.60	48.65	7.57
(21)	IPSL-CM5B-LR	1.16	3.12	62.41	5.97
(22)	MIROC-ESM	10.13	-1.16	74.04	3.43
(23)	MIROC-ESM-CHEM	10.01	x	75.05	x
(24)	MPI-ESM-LR	14.00	-1.82	89.63	10.92
(25)	MPI-ESM-MR	14.28	-2.00	80.00	11.30
(26)	MPI-ESM-P	13.36	-0.96	91.32	12.94
(27)	NorESM1-M	25.64	-2.20	57.93	13.61
(28)	NorESM1-ME	24.93	-2.40	75.58	9.78
(1-28)	**Mean**	**14.86(±5.12)**	**-1.92(±1.71)**	**76.53(±1.22)**	**6.10(±4.45)**
(A)	MERRA	15.22		108.05	
(B)	ERAI	14.98		89.85	
(C)	NOC	12.46		81.14	
(D)	BLEND	15.62		89.48	
(A-D)	**Mean**	**14.57(±1.43)**		**92.13(±9.82)**	

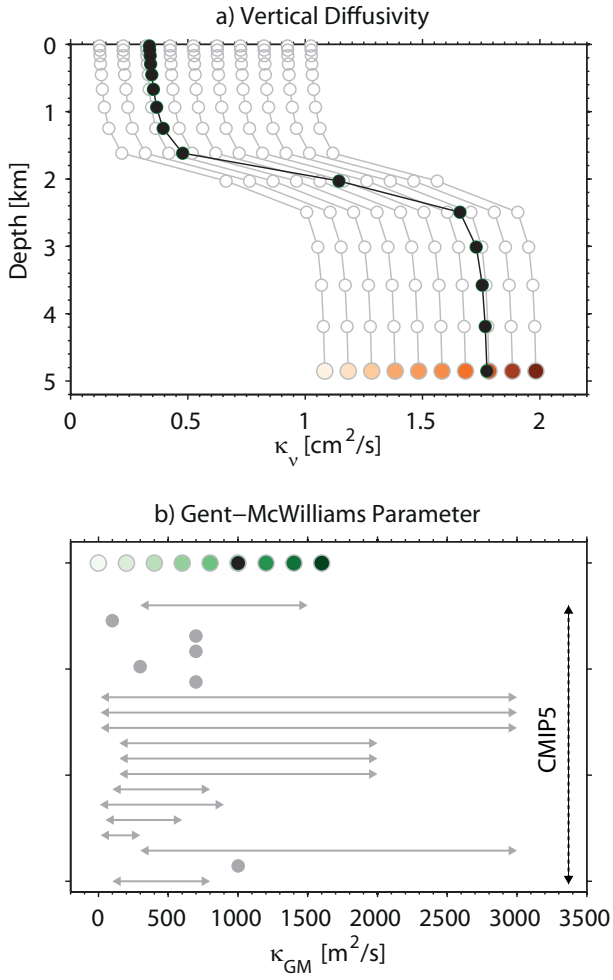

Figure 1. (a) MITgcm vertical diffusivity κ_ν depth-profile following *Bryan and Lewis* [1979] with the default profile of this study shown in black. We run a 10 member ensemble of the model in which we gradually increase the diffusivity by $\delta\kappa_\nu = 0.1$ cm^{2}s^{-1} uniformly over the domain's depth (see Sect. 2 of the main manuscript). (b) Thickness diffusion coefficient of the Gent-McWilliams eddy-parameterization κ_{GM} with default value of 1000 m^{2}s^{-1} (black). We perturb the parameter between 0–1600 m^{2}s^{-1} in a 9 member MITgcm-ensemble. A comparison with CMIP5 ensemble values taken from *Downes and Hogg* [2013] are shown as grey dots (where one value is given) or grey solid lines (where ranges are given or for a spatially dependent κ_{GM}).

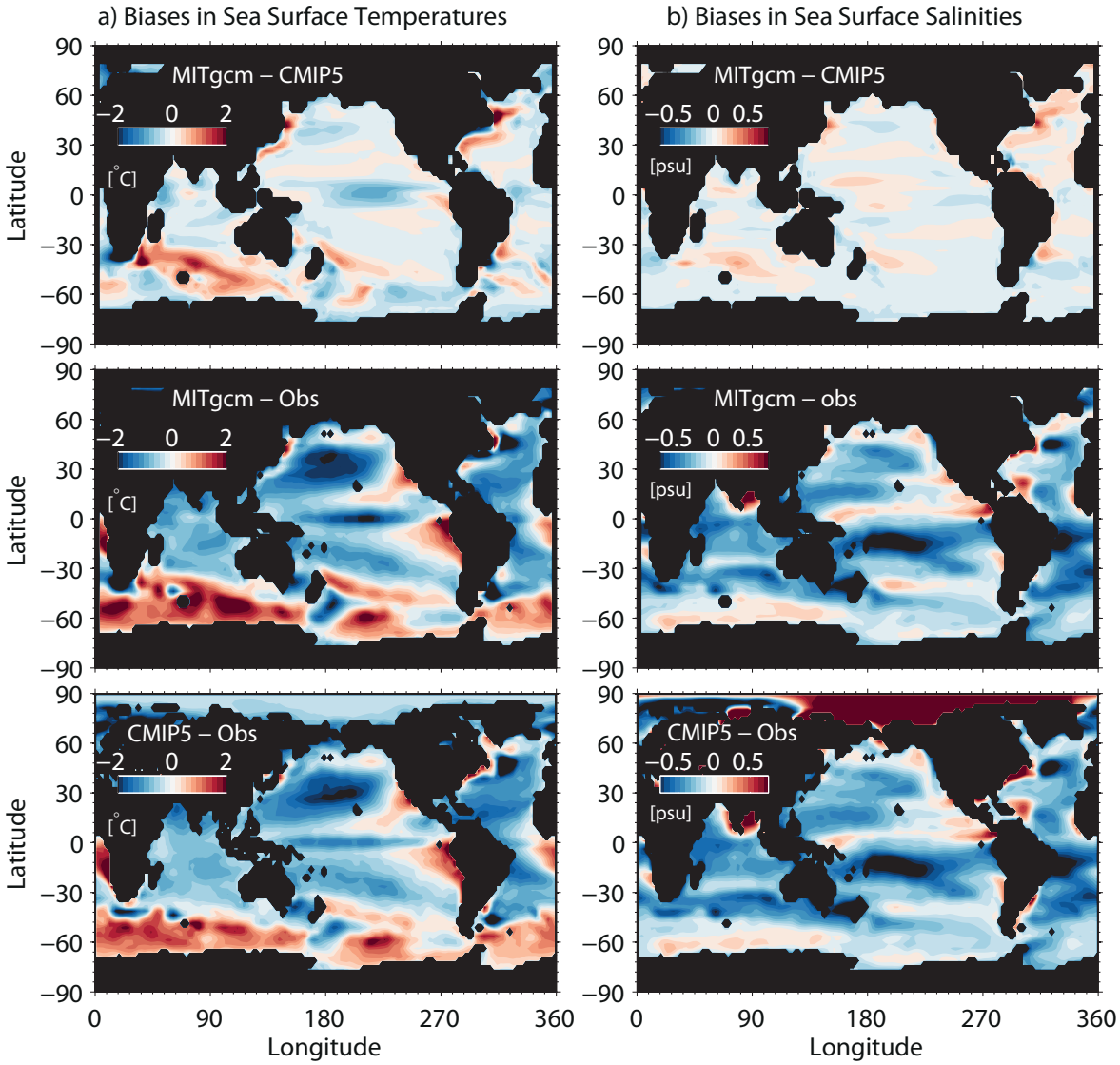

Figure 2. Biases in (a) Sea surface temperature (SST) and (b) sea surface salinity (SSS) of: (top panels) MITgcm-ensemble versus the CMIP5 coupled models, (middle panels) MITgcm-ensemble versus observations from *The World Ocean Atlas 2009* [*Locarnini et al.*, 2010; *Antonov et al.*, 2010], (bottom panels) CMIP5 ensemble versus observations.

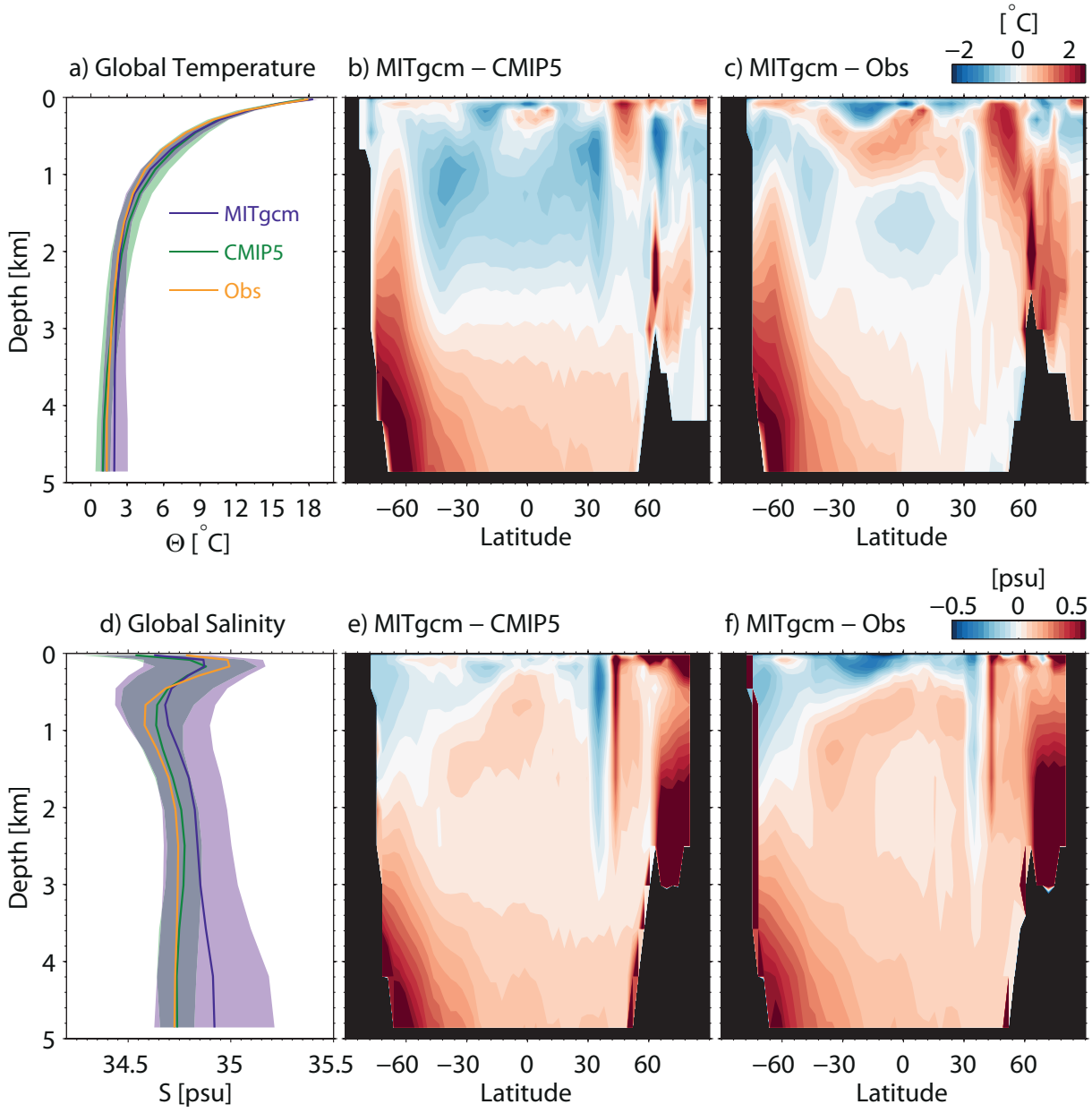

Figure 3. Globally averaged depth-profiles of (a) potential temperature and (d) salinity for the MITgcm-ensemble, the CMIP5 models and observations from *World Ocean Atlas 2009* [*Locarnini et al.*, 2010; *Antonov et al.*, 2010]. Solid lines are the mean and shadings are ± one standard deviation. The zonally-averaged ensemble-mean biases of the MITgcm-ensemble compared to (b, e) CMIP5 and (c, f) observations.

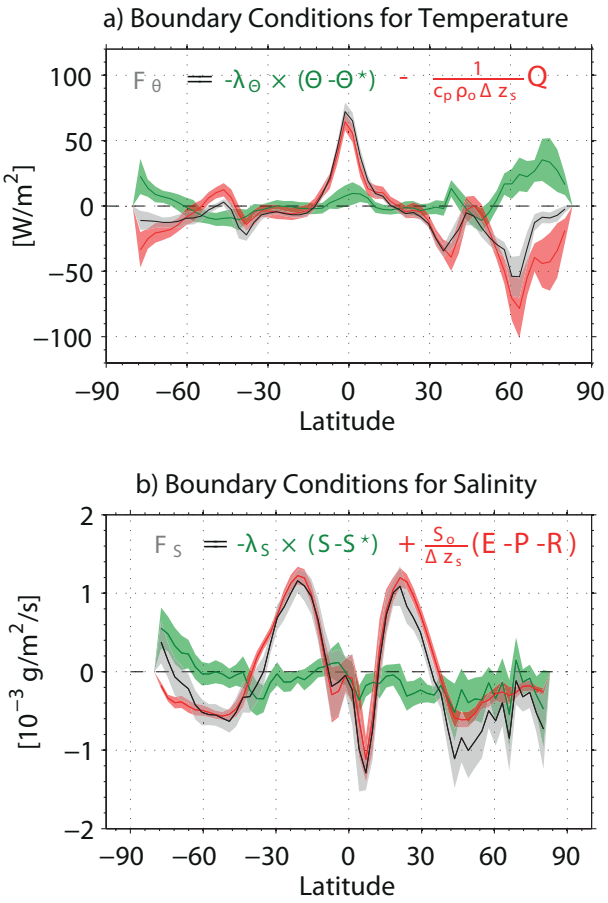

Figure 4. Boundary conditions (black) for (a) SST and (b) SSS with individual contribution of the relaxation terms (green) and surface buoyancy fluxes (red), refer to Eqns. 3–4 of the manuscript. Solid lines denote the MITgcm ensemble-mean and the shading indicates one standard deviation around the ensemble-mean.

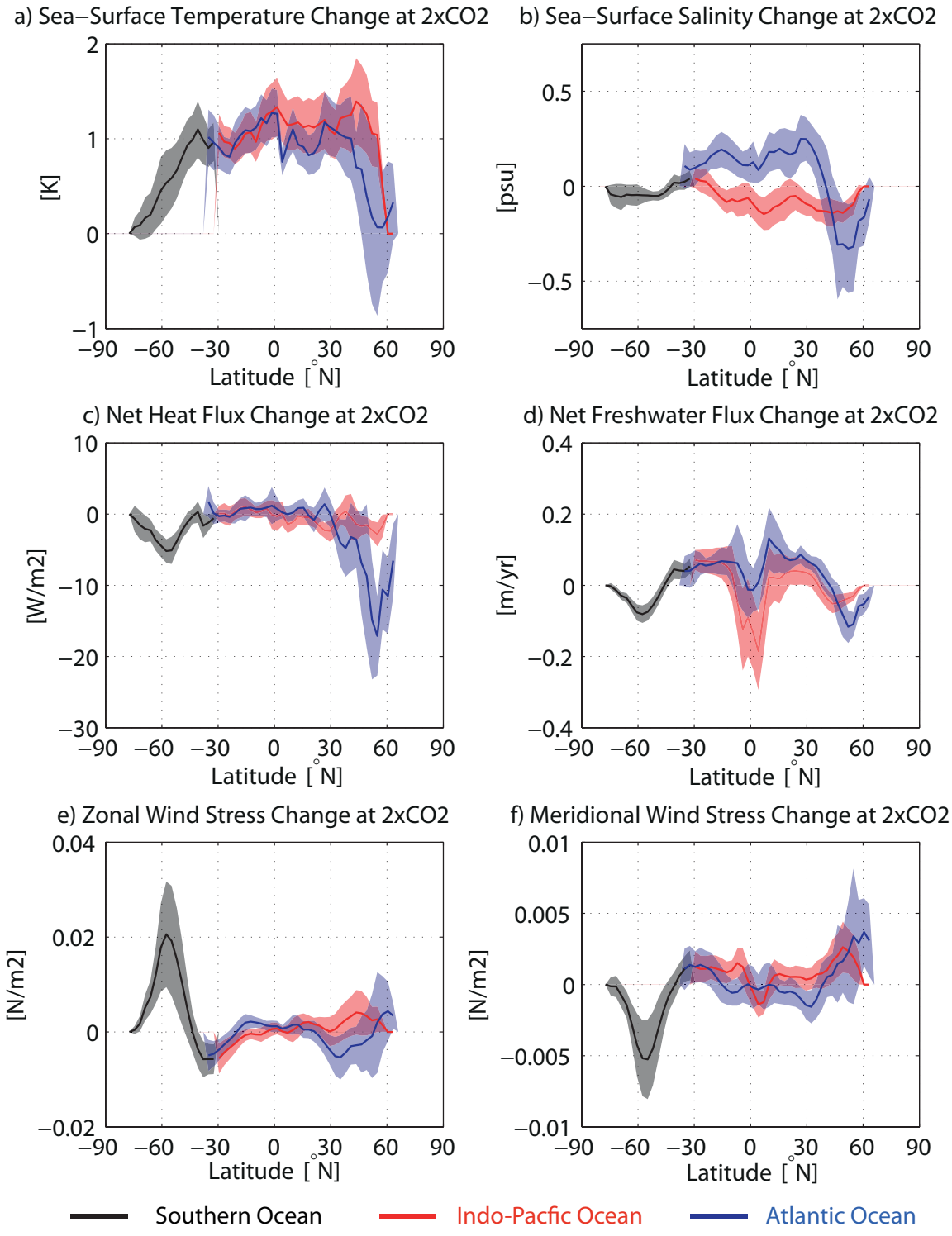

Figure 5. Change in sea-surface properties and air-sea fluxes under the transient 1%CO_2 scenario in the CMIP5 ensemble used to drive the MITgcm ocean model. Solid lines denote ensemble-mean and the shading indicates one standard deviation around the ensemble-mean.

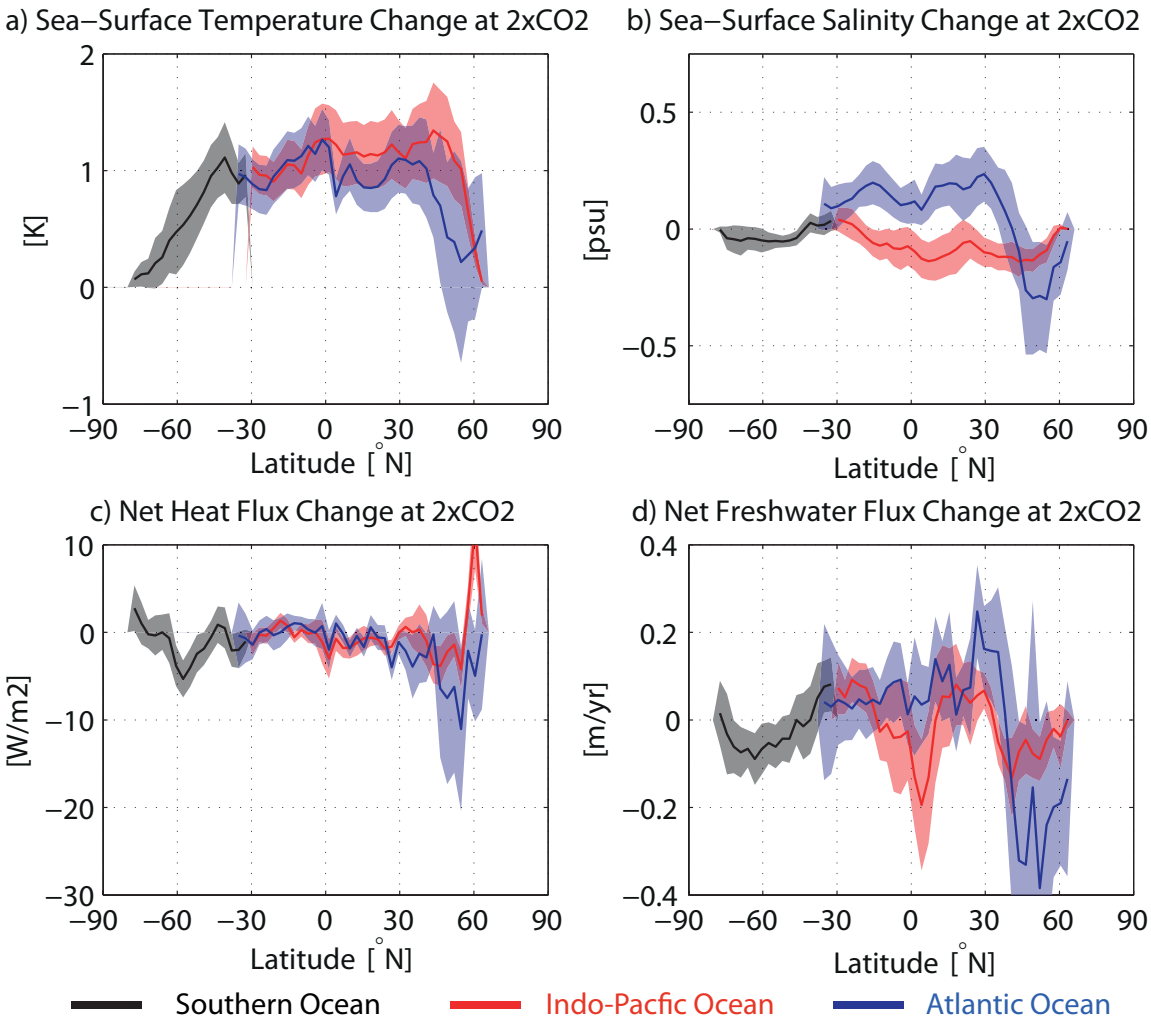

Figure 6. Similar to Fig. 5, but for the MITgcm ensemble.The fluxes shown are the effective fluxes calculated as the sum of the relaxation terms and the actual heat and freshwater fluxes from CMIP5 ensemble.

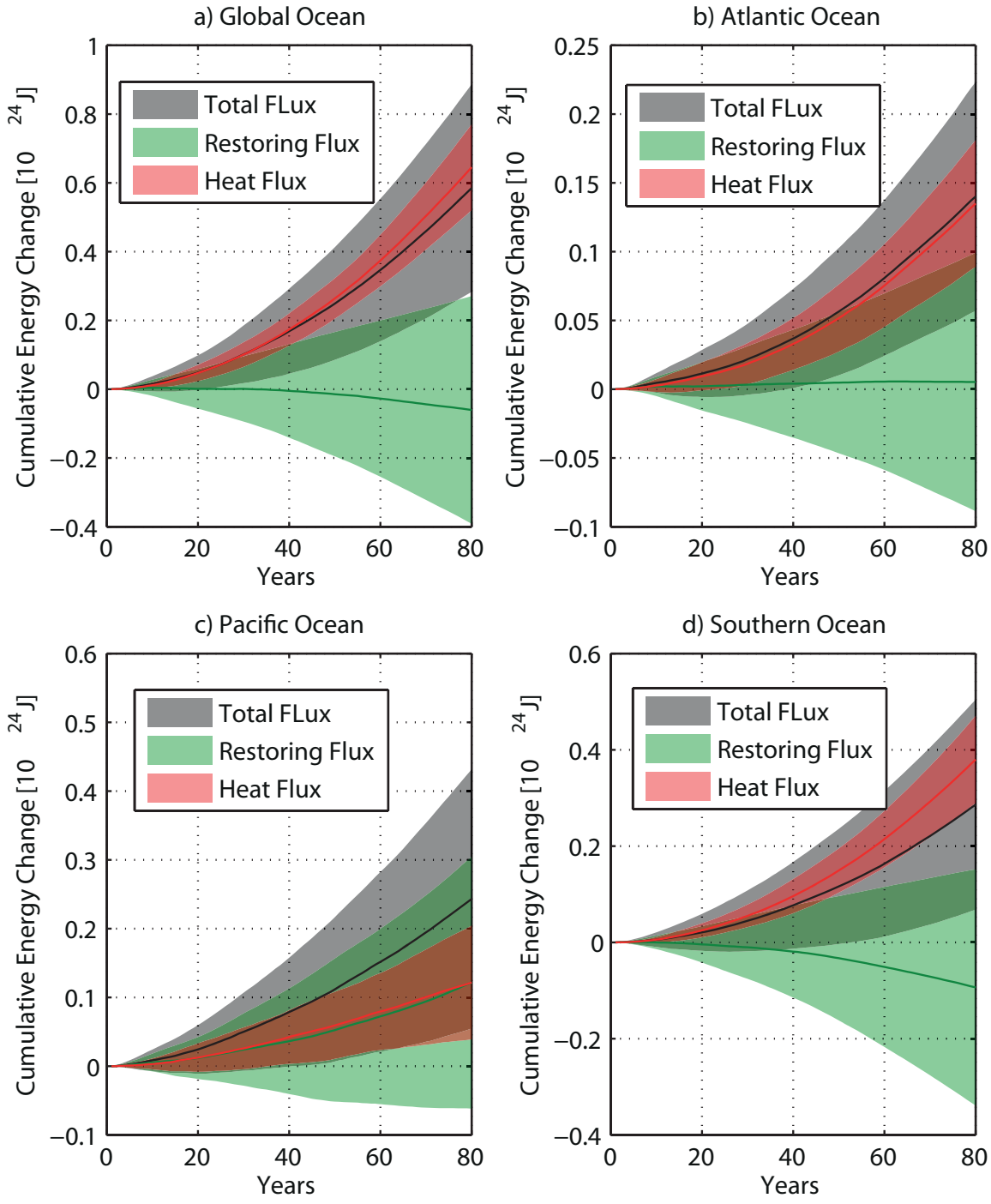

Figure 7. Cumulative energy change during the transient 1%CO_2 simulation in the MITgcm ensemble (black) and individual contributions from the relaxation terms (green) and CMIP5-derived heat fluxes (red). Solid lines denote ensemble-mean and the shading indicates one standard deviation around the ensemble-mean.

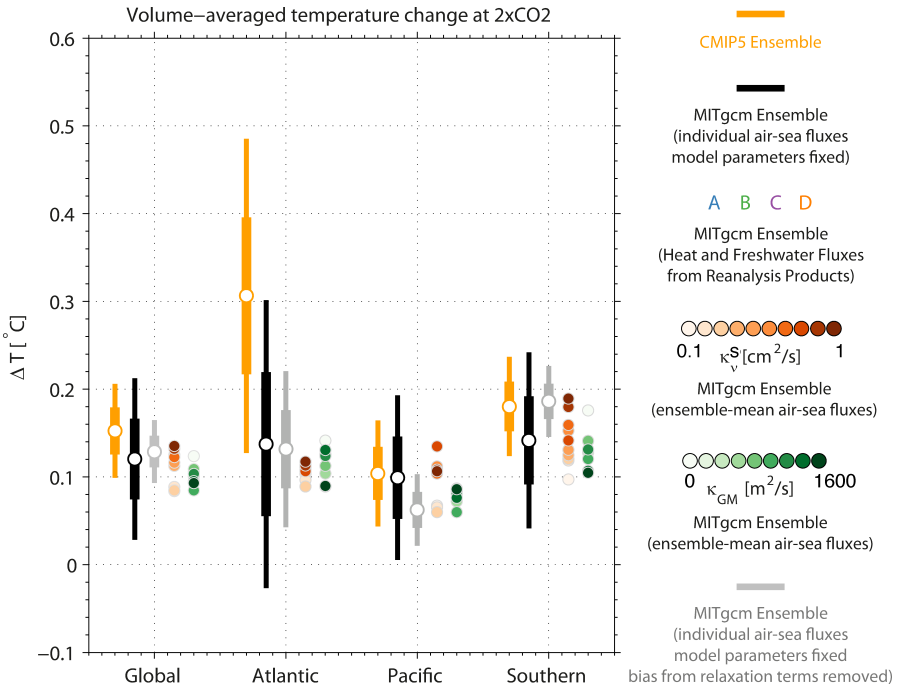

Figure 8. Volume-averaged temperature change in individual basins under the transient 1%CO_2 scenario. The color coding is similar to Fig. 4 of the manuscript, that is orange denotes the CMIP5 ensemble, solid black lines corresponding to the MITgcm ensemble forced with CMIP5 air-sea fluxes, red circles indicate the MITgcm ensemble in which the vertical diffusivity is varied, whereas the green circles indicate the MITgcm ensemble in which the eddy-related thickness diffusion is varied. The grey lines refer to the case where the impact of the restoring terms on the change in potential temperature are removed using the methodology introduced in Sect. 2 of the SM.

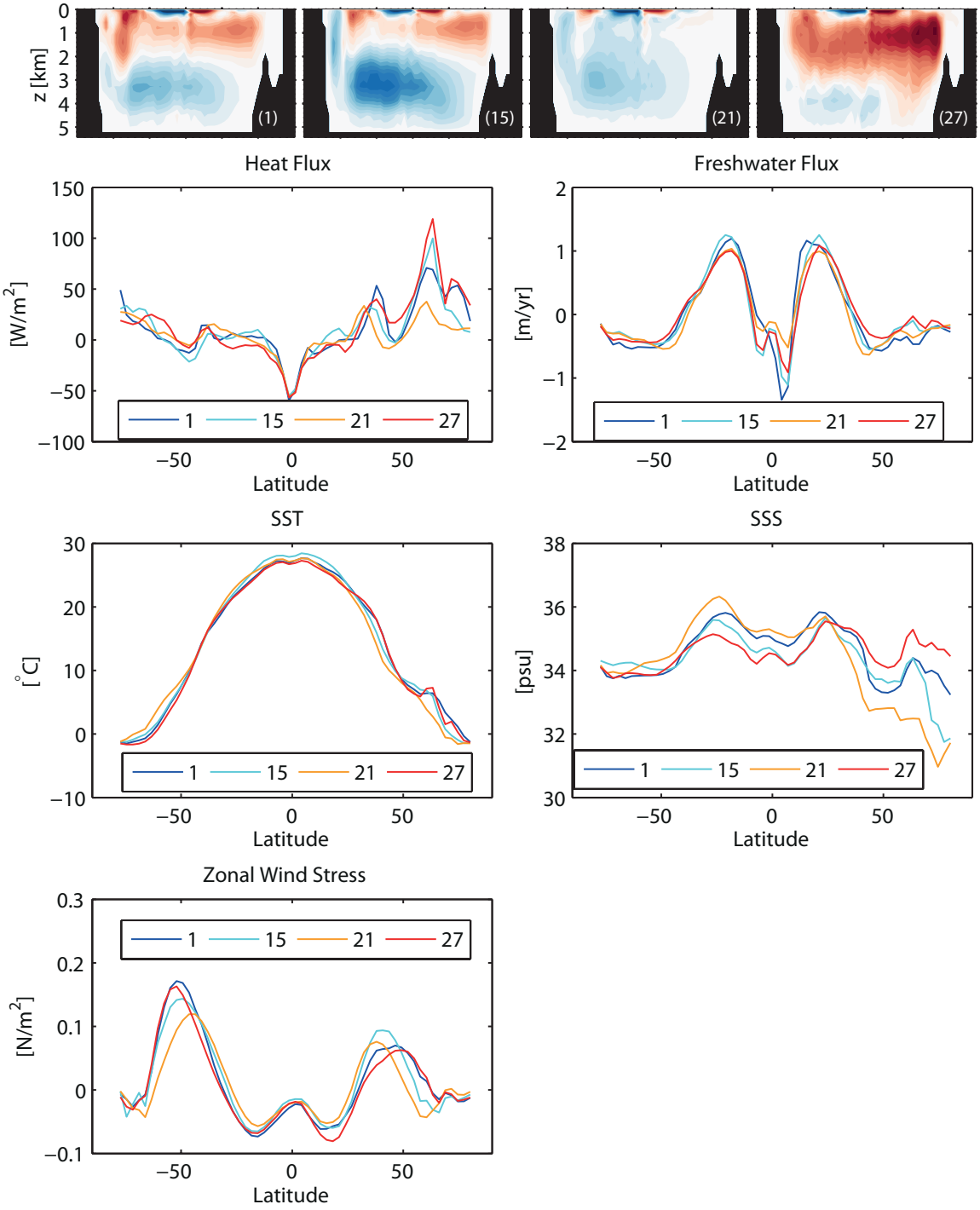

Figure 9. Top: Meridional overturning circulations (MOC) for four MITgcm ensemble-members described in the main text. In addition, we show the air-sea fluxes and surface fields for the same 4 ensemble-members below the MOC panels. The 4 members are selected to spread a wide range of ocean circulation and are shown to be driven by very different surface forcings (see text for explanation).

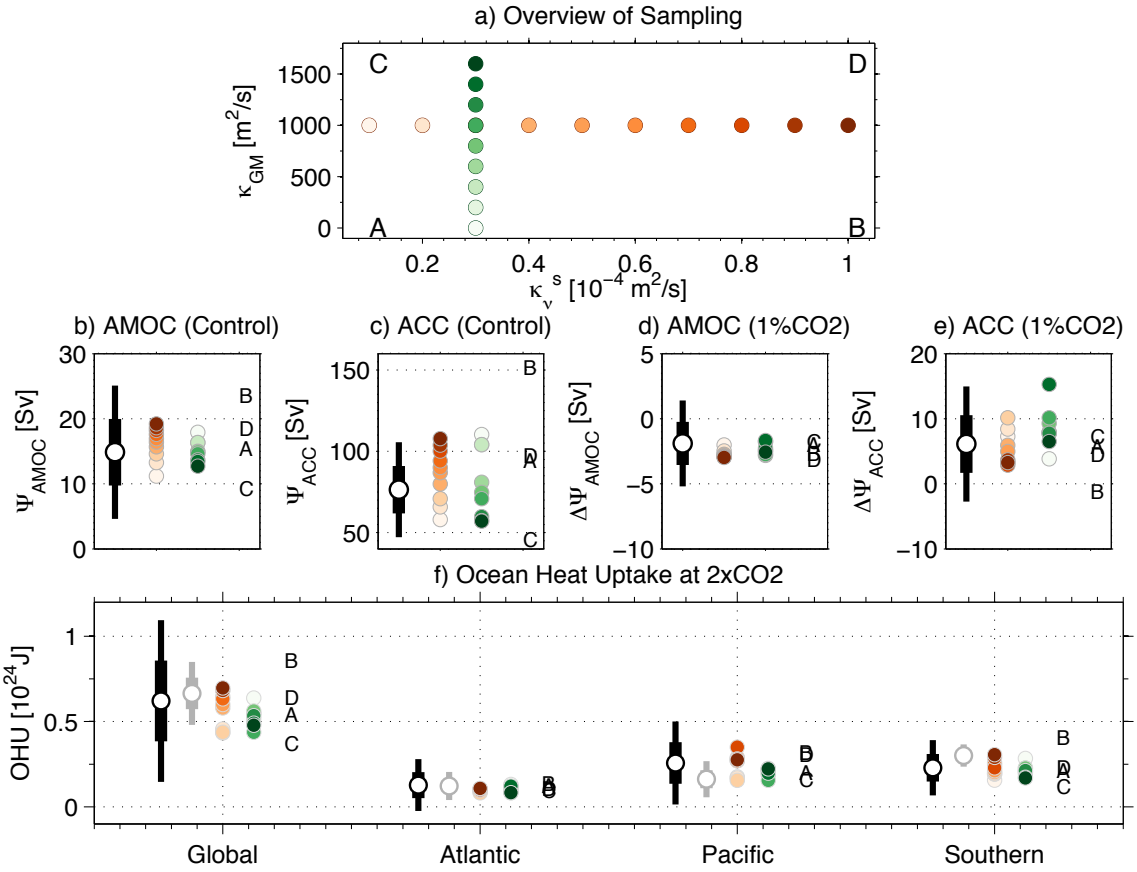

Figure 10. a) Sampling of the parameter space in surface vertical diffusivity (κ_ν^s) and eddy-related thickness diffusion (κ_{GM}). The combinations with minimum and maximum values of the two parameters are denoted as A,B,C and D. (b-c) Strength of the maximum meridional overturning in the Atlantic Ocean (AMOC) under pre-industrial conditions and under a 1%CO_2 warming scenario. (d-e) Strength of the volume transport of the Antarctic Circumpolar Current (ACC) under pre-industrial conditions and under a 1%CO_2 warming scenario. f) Basin-scale ocean heat uptake under a 1%CO_2 warming scenario.

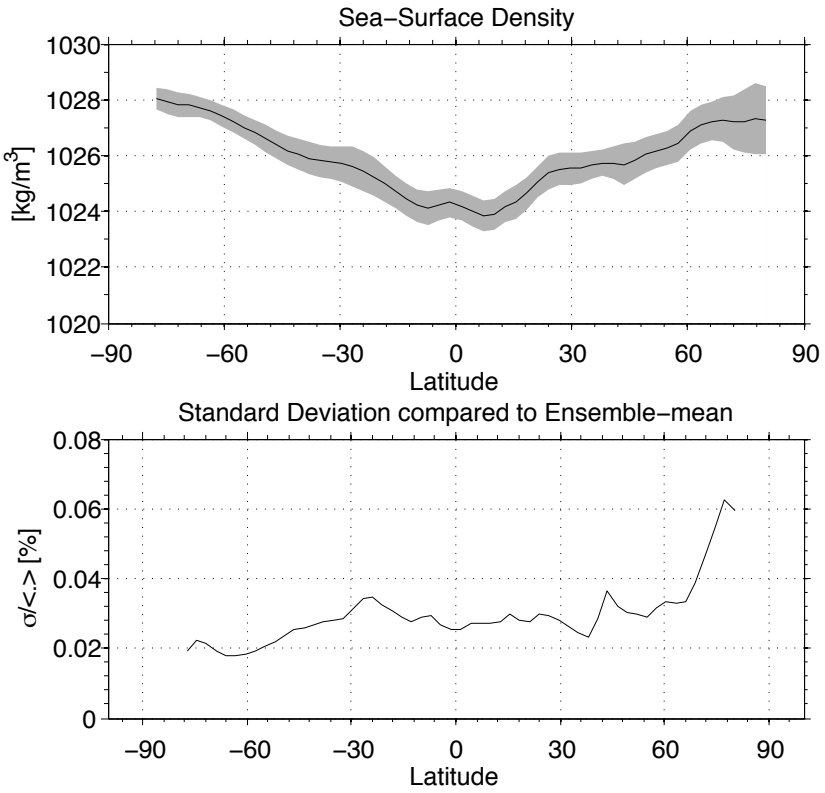

Figure 11. Based on the SST and SSS fields of the CMIP5 models depicted in Fig. 1 of the manuscript, this Figure shows the corresponding mean and spread across the ensemble for the surface density fields.